A genome-wide CRISPR screen identifies HuR as a regulator of apoptosis induced by dsRNA and virus

Huixin Gao[1,2,#], Yuxia Lin[1,2,#], Changbai Huang[1,2,#], Xiaobo Li[1,2], Michael S. Diamond[3], Chao Liu[1,4], Rong Zhang[5,*], and Ping Zhang[1,2,*]

[1]Key Laboratory of Tropical Diseases Control (Sun Yat-sen University), Ministry of Education, Guangzhou 510080, China;

[2]Department of Immunology, Zhongshan School of Medicine, Sun Yat-sen University, Guangzhou 510080, China;

[3]Departments of Medicine, Molecular Microbiology, Pathology & Immunology, Washington University School of Medicine, Saint Louis, MO, USA

[4] Department of Microbiology, Zhongshan School of Medicine, Sun Yat-sen University, Guangzhou 510080, China

[5]Key Laboratory of Medical Molecular Virology (MOE/NHC/CAMS), School of Basic Medical Sciences, Shanghai Medical College, Fudan University, Shanghai, 200032, China.

[#]These authors contributed equally to this work.

*To whom correspondence should be addressed:

Ping Zhang, zhangp36@mail.sysu.edu.cn;   Rong Zhang, rong_zhang@fudan.edu.cn

Summary Statement

Our study identified HuR as a regulator involved in the apoptosis induced by dsRNA or virus, and illustrated it acts through binding to *BCL2* mRNA and suppressing its translation.

Abstract

We performed an unbiased whole-genome CRISPR/Cas9 screen in A549 cells to identify potential regulators involved in cell death triggered by dsRNA. Of several top candidate genes, we identified the RNA binding protein *ELAV like protein 1* (*ELAVL1*) that encodes Hu antigen R (HuR). Depletion of HuR led to less cell death induced by dsRNA. HuR is mainly involved in the apoptosis, and all of its RNA recognition motifs are essential for its proapoptotic function. We further showed that the HuR depletion had no influence on the mRNA level of an anti-apoptotic gene, *BCL2*, instead downregulated its translation in a cap-independent way. Polysome fractionation studies showed that HuR retarded the *BCL2* mRNA in the non-translating pool of polysomes. Moreover, protection from dsRNA-induced apoptosis by HuR depletion required the presence of BCL2, indicating that the proapoptotic function of HuR is executed by suppressing BCL2. Consistently, HuR regulated apoptosis induced by infection of encephalomyocarditis or Semliki Forest virus. Collectively, our work identified a suite of proteins that regulate dsRNA-induced cell death, and elucidated the mechanism by which HuR acts as a pro-apoptotic factor.

Introduction

Programmed cell death (PCD) occurs after virus infections and often functions as a host defense strategy (Danthi, 2016; Orzalli and Kagan, 2017). Three major types of programmed cell death induced by virus infection have been documented: apoptosis, necroptosis, and pyroptosis (Danthi, 2016; Imre, 2020). Apoptosis is characterized by cell shrinkage, plasma membrane blebbing, DNA fragmentation, and chromosomal condensation. Apoptosis occurs via two distinct pathways, an intrinsic mitochondrial pathway regulated by BCL2 family members and an extrinsic pathway mediated by death receptors of the TNF family (Orzalli and Kagan, 2017). Necroptosis is a cell death characterized by cell swelling, plasma-membrane rupture, and release of cytosolic contents. The necroptosis pathway is mediated through receptor-interacting protein (RIP) kinases (Upton et al., 2017). Pyroptosis exhibits characteristics of both apoptosis and necroptosis. Pyroptosis is carried out by caspase-1, which mediates the maturation of proinflammatory cytokines such as IL-1 and IL-18, and gasdermin D (GSDMD). The GSDMD forms holes in the plasma membrane, eventually leading to cell death (Man et al., 2017).

Cell death can be triggered by virus attachment and entry, nuclei acids, or proteins (Danthi, 2016). dsRNA, as a common replication byproduct of both DNA and RNA viruses (Son et al., 2015), is a shared pathogen-associated molecular pattern that triggers cell death (Harashima et al., 2014; Jacobs and Langland, 1996; Kaufman, 1999) and cellular innate immune response (Takeuchi and Akira, 2009). Indeed, signaling through pattern recognition receptors including TLR3, RIG-I, and MDA5, can

promote cell death pathway signaling (Chattopadhyay and Sen, 2017; He et al., 2011; Hiscott et al., 2003). Interferons (IFNs), a downstream product of some pathogen detection sensing pathways, can promote the cell death by transcriptionally regulating the expression of key IFN stimulated genes (ISGs). Several ISG-encoded proteins, including protein kinases regulated by dsRNA (PKR) (Balachandran et al., 1998; Barber, 2005), 2,5-oligoadenylate synthetase (OAS) and RNase L (Castelli et al., 1998; Diaz-Guerra et al., 1997; Zhou et al., 1997), regulate cell death induced by dsRNA or virus infection (Chawla-Sarkar et al., 2003). Although ISG-induced cell death pathways are well understood, the molecular mechanisms underlying the dsRNA-induced cell death require further delineation.

To identify new regulators of virus-triggered cell death pathway, we performed a genome-wide CRISPR/Cas9-based gene editing screen, using a synthetic dsRNA analogue poly(I:C) as a stimulus. We focused study on *ELAVL1* (*HuR*), our top 'hit' for promoting dsRNA-induced cell death. *ELAVL1* (*HuR*) encodes for Hu antigen R (HuR), a member of Hu family protein that is ubiquitously expressed in many tissues (Hinman and Lou, 2008). HuR is an RNA binding protein comprised of three RNA recognition motifs (RRMs): RRM1 and RRM2 are contiguous, whereas the RRM (RRM3) is separated by a nucleocytoplasmic shuttling sequence. By regulating AU-rich element (ARE)-mediated mRNA stability and protein translation (Brennan and Steitz, 2001), HuR regulates multiple cellular processes, including tumorigenesis, stress responses, and programmed cell death (Hinman and Lou, 2008; Zhang et al., 2018). Although a context-dependent role of HuR in programmed cell death and survival has been defined in cancer (Hinman and Lou, 2008), the role of HuR in virus-induced apoptosis or survival remains unknown.

As part of our validation of HuR in promoting the cell death induced by dsRNA, we generated gene-edited cell lines lacking expression of HuR protein. Depletion of HuR resulted in less apoptosis induced by dsRNA. Mechanistically, HuR downregulated the expression of the anti-apoptotic protein BCL2, and the proapoptotic effect of HuR requires the presence of BCL2. Overall, our study shows that HuR is also involved in induction of apoptosis caused by encephalomyocarditis or Semliki Forest virus, two unrelated positive strand RNA viruses.

Results

A CRISPR/Cas9 screen for genes involved in the dsRNA-induced cell death

Transfection of poly(I:C) leads to rapid cell death in many human cell types (Harashima et al., 2014; Kibler et al., 1997). To identify cellular proteins involved in the cell death pathway induced by dsRNA, we performed a genome-wide CRISPR/Cas9 screen. A549 cells stably expressing Cas9 were transduced with the GeCKOv2 library targeting 19,050 human genes (Sanjana et al., 2014), with each gene targeted by six distinct single guide RNAs (sgRNAs), and enriched by puromycin selection. Stable sgRNA-expressing A549 cells were subjected to two rounds of poly(I:C) transfection, the second occurring seven days after the first to ensure all of the control, non-library transduced cells underwent death. We expanded the few surviving cells containing sgRNAs in culture and recovered their genomic DNA. We determined the targeted genes followed by PCR amplification and deep-sequencing of the sgRNAs from the integrated proviruses (**Fig. 1A**).

The top-ranking genes with statistically enriched sgRNAs were determined (**Fig. 1B**). As expected, genes in the type I IFN system including *RNASEL*, *JAK1*, and *STAT1/2* were at the top of the list, consistent with the established role of IFN signaling in modulating cell death (Barber, 2001). We also analyzed the functions of top 100 enriched genes by GOTERM, and classified them into ten distinct categories, including glycosaminoglycan biosynthetic process, host cell defense, and type I IFN signaling pathway, among others (**Fig. 1C**). Genes in the glycosaminoglycan biosynthetic process pathways (*SLC35B2*, *NDST1*, *B4GALT7*, *XYLT2*, and *B3GAT3*) were enriched in our screen, likely because glycosaminoglycans facilitate liposome attachment to cells, which enables delivery of poly(I:C) (Payne et al., 2007).

We chose representative genes from each clustered biological process and validated their effects on dsRNA-mediated cell death. Lentiviruses carrying individual sgRNAs were used to establish gene-edited A549 bulk cells. Cells expressing non-targeting sgRNAs served as a negative control, and sgRNA targeting *IFNAR* and *RNASEL* genes served as positive controls. The efficiency of gene editing was confirmed by qRT-PCR (**Fig. 1D**). The gene-edited bulk cells were transfected with poly(I:C) and cell viability was determined 24 h later using an MTT assay. The cell viability of poly(I:C)-transfected *IFNAR* or *RNase L* gene-edited cells were higher than control cells (**Fig. 1E**). The disruption of glycosaminoglycan biosynthesis pathway genes, including *B3GALT7*, *B4GLAT7*, *NDST7*, *SCL35B2*, or *XYLT2* (blue columns) also resulted in higher cell viability. Moreover, the cell viability of *ELAVL1* (*HuR*), *CAB39*, *CYFIP1*, *GATA6*, *OR8G5*, and *PDCD10*-edited cells was enhanced, which supports the data from our CRISPR/Cas9 screen.

HuR is required for the dsRNA-induced apoptosis

Based on the CRISPR/Cas9 screen data, we pursued *ELAVL1* (*HuR*) gene for further investigation, because it was a top 'hit' with five of six sgRNAs enriched (**Fig. 1B**). The *ELAVL1*-edited bulk cells were relatively resistant to poly(I:C)-induced cell death (**Fig. 1E**), although the protein encoded by *ELAVL1* (*HuR*), HuR is not known to regulate the virus-induced cell death. Upon dsRNA transfection, HuR protein was partially transported from nuclei to cytoplasm, implying it is actively enrolled in the cellular responses to dsRNA stimuli **(Fig. S1).** Then, we explored the functions of HuR in the cell death through loss-of-function strategy. Two HuR-knockout (KO) cell clones (HuR-KO1 and HuR-KO2) were selected from A549 and HeLa cell lines, and disruption of *ELAVL1* (*HuR*) gene was confirmed by western blotting and genomic DNA sequencing (**Fig. 2A and Fig. S2A**). The viability of control A549 or HeLa cells was ~20% at 24 h post transfection with poly(I:C), indicating that most cells did not survive (black columns, **Fig. 2B**). In contrast, the viability of all four KO cell clones was ~40%, about 2-fold higher than the control cells (white and grey columns, **Fig. 2B**). To confirm a role for HuR in dsRNA-induced cell death, we complemented the HuR-KO A549 cells by introducing a *ELAVL1-FLAG* fused to a fluorescent reporter gene. The Venus-positive HuR-complemented cells (HuR-RES) were sorted by flow cytometry. The HuR level in the HuR-RES cells was largely restored (**Fig. 2C**). At 24 h post transfection with poly(I:C), the extent of cell death in the HuR-RES cells was similar to control cells, but greater than in the HuR-KO cells (**Fig. 2D**). Most control and HuR-RES cells (~90%) showed characteristics of cell death including membrane blebbing, cell shrinkage, and cell detachment, similar

to control cells (**Fig. 2E**). In comparison, the morphological changes of HuR-KO cells were less severe than the control cells. These results demonstrate that HuR promotes the cell death induced by dsRNA.

To determine which type of cell death HuR contributed to, we evaluated cell viability in the presence of the inhibitors of apoptosis (z-VAD(OMe)-FMK, zVAD) or necroptosis (Necrostatin-1, Nec-1), or both inhibitors. Cell viability of the control and HuR-RES cells was enhanced by treatment of zVAD or zVAD+Nec-1 but not Nec-1 alone (**Fig. 2F**); in comparison, treatment with zVAD only slightly increased the cell viability of poly(I:C)-transfected HuR-KO cells. We also evaluated cleavage of poly ADP-ribose polymerase (PARP), a hallmark feature of apoptosis. Cleavage of PARP in poly(I:C)-transfected control cells was detected at 12 h and increased at 24 h. In the poly(I:C)-treated HuR-KO cells, levels of PARP cleavage were lower than in control cells (**Fig. 2G**). In addition, we tested whether pyroptosis occurs in A549 cells upon dsRNA treatment by using VX765, an inhibitor of caspase-1 which is a principle effector protease of pyroptosis (Wannamaker et al., 2007). A549 cells were transfected with poly(I:C) in the presence of vehicle (DMSO) or VX765. VX765 treatment did not alter the morphological changes and cell viabilities (**Fig. S3A and 3B**), indicating pyroptosis barely occurs in the dsRNA-triggered A549 cells. Overall, these results suggest that HuR mainly regulates the apoptosis pathway of cell death induced by dsRNA.

Moreover, we examined whether HuR plays a role in the apoptosis induced by other classic stimuli, including hydrogen peroxide, doxorubicin, and staurosporine. Upon hydrogen peroxide stimulation, a large proportion of control cells underwent apoptosis, while the viability of HuR-KO cells was significantly higher (**Fig. S4A and S4B**). In contrast, upon treatment with doxorubicin or staurosporine,

PARP cleavage levels in HuR-KO were slightly increased than control cells (**Fig. S4C and 4D**), indicating HuR plays differential roles in the apoptosis induced by different stimuli.

All three domains of HuR are required for its proapoptotic function

To evaluate role of individual domain of HuR in mediating its proapoptotic activity, we generated bulk cells expressing truncated HuR lacking RRM1 (ΔRRM1), RRM2 (ΔRRM2), or RRM3 domain (ΔRRM3) in HuR-KO cells (**Fig. 3A**). Western blotting data confirmed that all three HuR truncates were expressed (**Fig. 3B**). Upon treatment with poly(I:C), control and HuR-RES cells showed severe characteristics of cell death including membrane blebbing, cell shrinkage, and cell detachment (**Fig. 3C**). The morphological changes of ΔRRM1, ΔRRM2, and ΔRRM3 cells were less severe than control cells, and were comparable to HuR-KO cells (**Fig. 3C**). The cell viabilities were measured using MTT assay. As expected, the viability of HuR-RES cells was significantly lower than HuR-KO cells. In contrast, the viabilities of ΔRRM1, ΔRRM2, and ΔRRM3 cells were higher than the control cells, and were comparable to HuR-KO cells, (**Fig. 3D**), suggesting that all three RRM domains of HuR are required for mediating cell death. The cleaved PARP levels in HuR-KO cells, ΔRRM1, ΔRRM2, and ΔRRM3 cells were comparable, and lower than control and HuR-RES cells (**Fig. 3E**). Deletion of each individual RRM domain of HuR was sufficient to impair the pro-apoptotic activity of HuR, suggesting that all three RRM domains are required for the dsRNA-induced apoptosis regulated by HuR.

HuR inhibits the translation of *BCL2*

Given an important function of HuR is to stabilize target gene expression at the transcriptional level (Brennan and Steitz, 2001), we performed a RNA sequencing (RNA-seq) assay to define genes transcriptionally altered by HuR expression. However, we did not identify any apoptosis-related genes among the top-ranked list, implying that HuR might not promote the dsRNA-induced apoptosis by regulating the mRNA levels of apoptosis-related genes (**Fig. S5**). We then explored whether HuR regulates expression of apoptosis-related genes. As the mRNA stability and translation of *BCL2* was regulated by HuR (Ishimaru et al., 2009), we compared protein levels of BCL2 in control, HuR-KO, HuR-RES, ΔRRM1, ΔRRM2, and ΔRRM3 cells. Notably, the protein levels of the BCL2 in HuR-KO cells were markedly increased compared to the control and HuR-RES cells. Similarly, the BCL2 level in the ΔRRM1, ΔRRM2, and ΔRRM3 cells was higher than in control cells (**Fig. 4A**).

As HuR binds to the *BCL2* mRNA *in vitro* and in HL60 cells (Ishimaru et al., 2009), we examined whether HuR is also associated with *BCL2* mRNA in A549 cells by RNA immunoprecipitation (RIP) assay. The mRNA levels of negative control *GAPDH* were comparable in the HuR-KO and HuR-RES A549 cells, while positive control *β-actin* mRNA level in the HuR-RES cells was higher than the HuR-KO cells (Dormoy-Raclet et al., 2007) (**Fig. 4B**). The *BCL2* mRNA levels associated with HuR in HuR-RES cells was significantly higher than HuR-KO cells, suggesting that HuR binds to *BCL2* mRNA in A549 cells.

As HuR knockout led to higher level of BCL2 protein, we first tested whether HuR regulates the mRNA level of *BCL2*. To this end, the *BCL2* mRNA levels in control, HuR-KO, HuR-RES, ΔRRM1, ΔRRM2, and ΔRRM3 cells were compared. Loss of expression of full length or truncated HuR did not impact on the overall cellular levels of *BCL2* mRNA (**Fig. 4C**), which is consistent with our RNA-seq data and suggests that HuR does not affect transcription of *BCL2* gene in A549 cells. Next, we examined whether HuR regulates the stability of *BCL2* mRNA by using actinomycin D to block the cellular transcription. At indicated time points, total RNA was prepared for qRT-PCR to measure mRNA levels of *BCL2* or *COX-2*, the latter a known target gene stabilized by HuR (Sengupta et al., 2003). As expected, the levels of *COX-2* mRNA decreased more rapidly in HuR-KO cells than in control cells. In contrast, the *BCL2* mRNA levels were similar in control and HuR-KO cells at all time points (**Fig. 4D**), suggesting that HuR does not affect the *BCL2* mRNA stability in A549 cells.

To investigate whether HuR regulated the translation of BCL2, we evaluated the association of *BCL2* mRNA with translating ribosomes by polysome profiling assay. Whole cell extracts were subjected to sucrose density gradient centrifugation, and the *BCL2* mRNA levels in each ribosome fraction were measured by qRT-PCR. The *BCL2* mRNA in control cells was distributed mainly in low molecular weight polysomes (gradient top, fractions 1-7, **Fig. 4E**); however, this was shifted to high molecular weight translating polysomes (gradient bottom, fractions 9-12) in HuR-KO cells (**Fig. 4E**). The distributions of control *GAPDH* mRNAs were similar in the two cell lines. This result indicates that HuR depletion leads to a redistribution of *BCL2* mRNA from non-translating polysomes to translating polysomes, thereby increasing its rate of translation.

Considering HuR regulates the cap-independent translation of various genes directed by IRES (Kullmann et al., 2002; Winkler et al., 2014), HuR might regulate the *BCL2* translation in a similar way. To test this possibility, we compared whether the BCL2 protein level is affected by rapamycin, an inhibitor of cap-dependent translation. Cells were transfected with poly(I:C) in the presence of DMSO or rapamycin, and harvested at 24 h post transfection. The incubation of rapamycin did not affect the protein levels of BCL2 in both control and HuR-KO cells (**Fig. 4F**), suggesting that HuR regulates the BCL2 translation in a cap-independent way.

We further tested whether HuR affects the post-translational degradation of BCL2 using inhibitors of two major protein degradation pathways, MG132 (blocks proteasome degradation) and NH$_4$Cl (blocks lysosomal degradation). Treatment with MG132 or NH$_4$Cl did not alter the protein levels of BCL2 in control and HuR-KO cells (**Fig. 4G**), indicating that the reduction of BCL2 protein levels mediated by HuR was independent of proteasome and autophagy mediated degradation.

BCL2 plays an essential role in mediating the proapoptotic effect of HuR

To explore whether BCL2 plays a role in the proapoptotic action of HuR, we utilized a highly selective inhibitor of BCL2, Venetoclax (Ashkenazi et al., 2017). Cells were stimulated with poly(I:C) in the presence of Venetoclax ranging from 0 to 4 μM, and cell viability was measured at 24 h post transfection. As shown in **Fig. 5A**, the cell viability of all tested cells gradually decreased with increasing Venetoclax concentrations, indicating a protective role of BCL2 in the dsRNA-induced apoptosis. When treated with 1 μM Venetoclax, the cell viability of HuR-KO cells was higher than the

control and HuR-RES cells, whereas cell viability of HuR-KO cells was closer to the other two cells in the presence of 2 μM Venetoclax. Treatment of 4 μM Venetoclax resulted in similar low percentages of cell viability (under 10%) in all three cells (**Fig. 5A**). Treatment of Venetoclax alone did not affect the cell viability (**Fig. S6A**). In addition, we examined whether other anti-apoptotic proteins, such as Bcl-XL and Mcl-1 are involved in the HuR-regulated apoptosis by using their specific inhibitors (WEHI-539 against Bcl-XL and S63845 against Mcl-1). Our data showed that treatment of either WEHI-539 or S63845 did not alter the cell viabilities of control and HuR-KO cells, ruling out the involvement of Bcl-XL and Mcl-1 in the dsRNA-induced apoptosis (**Fig. S6B**).

To validate that BCL2 mediates the proapoptotic effect of HuR, we further generated two gene-edited cells: *BCL2* KO cells (BKO), as well as *HuR* and *BCL2* double knockout cells (dKO). Disruption of *BCL2* or *HuR* gene in BKO and dKO cells was confirmed by western blot and sequencing (**Fig. 5B and Fig. S2B**). As expected, the viability of BCL2-KO cells was lower than control cells (**Fig. 5C**). Knockout of BCL2 in addition to knockout of HuR (*i.e*., dKO cells) resulted in lower cell viability than HuR-KO alone (**Fig. 5C**). The BCL2-KO cells showed more severe morphological changes after poly(I:C) transfection than the other three cells, with greater cell shrinkage and loss of adherence (**Fig. 5D**). Then the whole cell lysates were collected for western blot. As shown in **Fig. 5B**, PARP cleavage dramatically decreased in poly(I:C)-treated HuR-KO cells compared to control cells. In line with this, BCL2 protein was markedly increased in HuR-KO cells compared to the control cells, consistent with the observation in Fig. 4A. In contrast, PARP cleavage was markedly increased in BKO cells than control cells, suggesting the anti-apoptotic activity of BCL2. As expected, the PARP cleavage in dKO

cells was increased than that in HuR-KO cells, suggesting that HuR promotes poly(I:C)-induced apoptosis through BCL2. Collectively, these results suggest that the pro-apoptotic effect of HuR is mediated in part by BCL2.

HuR promotes apoptosis triggered by virus infection

To explore whether HuR confers a pro-apoptotic activity in the context of virus infection, two single-stranded, positive-sense RNA viruses (encephalomyocarditis virus [EMCV] and Semliki Forest virus [SFV]) were employed, as they produce dsRNA during infection and trigger apoptosis (Bauernfried et al., 2020; El Maadidi et al., 2014; Iordanov et al., 2005; Scallan et al., 1997; Urban et al., 2008). The control and HuR KO cells were inoculated with EMCV or SFV at a multiplicity of infection (MOI) of 1. qRT-PCR analysis at 3, 6, 9, and 12 h post-infection (hpi) showed comparable viral RNA levels between control and HuR KO cells (**Fig. 6A**), indicating that HuR depletion does not alter viral replication. Next, we used morphological observation, flow cytometry, and western blot analysis to measure apoptosis. Microscopic images showed that after EMCV or SFV infection, the majority of control cells showed typical characteristics of cell death, including cell membrane blebbing and cell detachment, whereas more HuR-KO cells remained intact. In response to either EMCV or SFV infection, a large proportion of BKO cells underwent shrinkage and cytoplasmic blebbing, and cellular morphological change of dKO cells was more severe than HuR-KO (**Fig. 6B**). The flow cytometry data showed that after virus infection around 30% and 35% of control cells underwent apoptosis at 24 h p.i., whereas only around 12% and 15% of HuR KO cells were apoptotic (**Fig. 6C**). In response to either

EMCV or SFV infection, the levels of PARP cleavage in the BKO cells were the highest among these cells. The cleaved PARP level in the dKO cells was lower than BCL2-KO cells, but higher than HuR-KO cells (**Fig. 6D**), suggesting that the proapoptotic effect of HuR requires the presence of BCL2.

Discussion

Cell death elicited by viral infection affects the interplay between host and virus. In this study, we identified that HuR, an "old" regulator of apoptosis in cancer, plays a "new" role in regulating the virus-triggered apoptosis. Our work also illustrated the mechanistic basis of HuR functions: by binding the mRNA of *BCL2* and suppressing its translation.

Our CRISPR/Cas9 screen showed that the top 100 genes from the screen were clustered in many biological processes including the type I IFN signaling pathway which is known to play a role in cell death, confirming that our screen was robust and reliable. We validated and then investigated the function of one of the top hits, *HuR* in this study. The disruption of *HuR* gene led to lower cell death. Conversely, complementation of *HuR* in HuR-KO cells restored the extent of cell death induced by dsRNA. DsRNA triggers three main types of cell deaths, namely apoptosis, necroptosis, and pyroptosis in different cells (Danthi, 2016; Imre, 2020). Our study using the inhibitor of caspase-1 indicated that pyroptosis does not occur in dsRNA-transfected A549 cells (Fig. S3), in line with the notion that pyroptosis mainly occurs in immune cells mediating inflammatory responses (Galluzzi et al., 2018).

Moreover, neither apoptosis inhibitor nor necroptosis inhibitor could fully recover the cell viability (Fig. 2F), suggesting that A549 cells undergo multiple types of cell death such as apoptosis, necroptosis, or autophagy. Our data gathered from inhibitor assay, western blot, and morphological observation demonstrated that HuR is mainly involved in the apoptosis induced by dsRNA. As pyroptosis does not occur, the PARP cleavage in poly(I:C)-treated cells was mediated by caspases in the apoptosis pathway (Erener et al., 2012). Interestingly, HuR also confers a pro-apoptotic activity in response to hydrogen peroxide, but not to doxorubicin or staurosporine, in keeping with previous studies (Badawi et al., 2018; Winkler et al., 2014). HuR plays differential roles in the apoptosis under different contexts, implying that multiple apoptosis signaling pathways, HuR-dependent or HuR-independent, are employed by cells.

The proapoptotic effect of HuR does not appear to rely on the IFN signaling pathway, as the HuR depletion barely affected the levels of *IFN-β* and ISG genes. Also, HuR barely affects the mRNA levels of apoptosis-related genes, indicating that its regulatory action is not executed through stabilizing mRNA of apoptosis-related genes.

Our work showed that in A549 cells, HuR binds to the mRNA of *BCL2*, which encodes an antiapoptotic protein, consistent with a previous report (Ishimaru et al., 2009). Lacking of each HuR domain could not restore its pro-apoptotic ability, implying that the RNA binding activity is crucial. Intriguingly, the association of HuR to *BCL2* mRNA does not regulate its transcription, but negatively regulate its translation in an IRES-directed cap-independent way, which differs from the observations gathered from other cells. In HL60 cells, HuR promotes both *BCL2* mRNA stability and translation (Ishimaru et al., 2009); in 293T cells, HuR knockdown led to a decrease of endogenous BCL2

expression, but an increase of a BCL2-ARE-reporter transcription, suggesting HuR has opposite effects on endogenous and ectopic BCL2 ARE (Ghisolfi et al., 2009). Therefore, we proposed although HuR binding to BCL2 mRNA is commonly found in many cell types, its regulation on *BCL2* transcription and translation is cell-specific, directing different levels of BCL2 in different cells, and thereby different phenotypes under physiological stresses.

Our work reveals BCL2 is one of major mediators involved in the pro-apoptotic effect of HuR. The inhibition of BCL2 by a specific inhibitor or disruption of the *BCL2* gene increased the vulnerability of A549 cells to cell death upon dsRNA transfection, consistent with idea that BCL2 is protective against dsRNA-induced cell death (Diaz-Guerra et al., 1997; Domingo-Gil and Esteban, 2006). In the absence of BCL2, the pro-apoptotic effect of HuR was largely diminished, indicating that BCL2 likely mediates the pro-apoptotic function of HuR. Notably, HuR not only binds to *BCL2* mRNA, but also interacts with BCL2 protein (Ghisolfi et al., 2009), adding another layer of complexity between HuR and BCL2.

We also demonstrated that HuR contributes to the apoptosis triggered by two RNA viruses, EMCV and SFV. Both EMCV and SFV can produce dsRNA during replication, leading to apoptosis of *in vitro* cells (El Maadidi et al., 2014; Iordanov et al., 2005; Scallan et al., 1997; Urban et al., 2008) and *in vivo* mice (Chattopadhyay et al., 2011). Our study revealed that A549 cells also underwent apoptosis upon infection with EMCV or SFV. As BCL2 overexpression allowed survival of SFV-infected cells (Scallan et al., 1997), we propose that the upregulated BCL2 levels in HuR-KO partially contributes to the lower apoptosis extent induced by SFV infection. To be noted, HuR might also regulate the apoptosis in a BCL2-independent way, as the apoptosis extent was not fully restored in the virus-infected dKO cells

(Fig. 6D, lane 8). Nonetheless, HuR does not have a pro-apoptotic role in the cell death caused by Dengue virus, VSV, and Sendai virus (data not shown), which might be explained by these viruses trigger cytolysis via non-dsRNA factors. For example, viral proteins of DENVs including capsid protein, NS2A, and NS2B3/NS3, rather than dsRNA, are the main stimuli of apoptosis (Okamoto et al., 2017).

In summary, our CRISPR/Cas9 screen identified proteins that regulate dsRNA-triggered cell death. In response to dsRNA or viral infection, HuR is transported into cytoplasm, binding to BCL2 mRNA and blocking its translation, eventually promoting the apoptosis. These findings underscore the significance of the association between HuR and BCL2 mRNA, and illustrate a new role of HuR in the apoptosis induced by virus.

Materials and methods

Cells and reagents

Human lung carcinoma epithelial cells (A549, ATCC CCL-185), human cervical cancer cells (HeLa, ATCC CCL-2) and human embryonic kidney cells (293T, ATCC CRL-3216) were maintained in Dulbecco Modified Eagle Medium (DMEM) (Gibco, South America, USA) supplemented with 10% fetal bovine serum (FBS) (Gibco) at 37 °C with 5% CO_2. Baby hamster kidney cells (BHK21, ATCC CCL-10) and African green monkey kidney cells (Vero, ATCC CCL-81) were maintained in DMEM supplemented with 5% FBS at 37 °C in an incubator with 5% CO_2. *Aedes albopictus* cells (C6/36, ATCC CRL-1660) were maintained in DMEM (Gibco) supplemented with 10% FBS (Gibco) and NEAA

(Gibco) at 28 °C in an incubator with 5% CO_2. The media were supplemented with 100 units/ml of streptomycin and penicillin (Invitrogen, California, USA).

Inhibitor of apoptosis, z-VAD(OMe)-FMK (MCE), and inhibitor of necrosis, Necrostatin-1 (MCE), were dissolved in DMSO at a stock concentration of 100 mM. Inhibitors of Bcl-XL (WEHI-539) and inhibitor of Mcl-1 (S63845) were dissolved in DMSO at a stock concentration of 10 mM. Inhibitor of cap-dependent translation, rapamycin (MCE), were dissolved in DMSO at a stock concentration of 10 mM.

CRISPR/Cas9 genetic screen

The GeCKO v.2 human CRISPR pooled libraries (A and B) encompassing 123,411 different sgRNA targeting 19,050 genes were purchased from GenScript. Lentiviral production was prepared independently for each half-library in HEK293FT cells by co-transfecting sgRNA plasmids with psPAX2 and pCMV-VSV-G at a ratio of 4:3:1 with FuGENE HD (Promega, Wisconsin, USA). After 2 days, culture supernatants were passed through a 0.45 μm filter, and used for gene transduction. A549 cells were transduced with each CRISPR-sgRNA lentiviral library at an MOI of 0.3 and a coverage of 500× for sgRNA representation. Cells were selected with puromycin for 8 days and expanded. Then, 6 x 10^7 cells from each library were pooled and transfected with poly(I:C) using Lipofectamine 2000 (Invitrogen). After 7 days, cells were re-transfected with poly(I:C) for a second round. A complete poly(I:C)-induced cell death was observed in control cells at 7 days post 2nd transfection. Surviving cells were collected at 7 days post-transfection for genomic DNA extraction using a QIAamp DNA column

(Qiagen, Hilden, Germany). The inserted sgRNAs were amplified and sequenced using next-generation sequencing on an Illumina MiSeq (Plateforme MGX, Institut Génomique Fonctionelle). The sgRNA sequences were analyzed using the MAGeCK software and the RIGER software (Jeong et al., 2019; Li et al., 2014).

Generation of bulk gene-edited cells

Gene-edited cell clones were generated using the CRISPR/Cas9 system. sgRNAs for the top-ranking genes were individually cloned into the plasmid lentiCRISPR v2 (Addgene #52961). sgRNAs were listed in **Table S1**. LentiCRISPR v2 containing sgRNA, pSPAX2 (Addgene #12260), and pMD2.G (Addgene #12259) were introduced into 293T cells using FuGENE® HD Reagent (Promega). After 2 days, culture supernatants were passed through a 0.45 µm filter, and used for gene transduction. A549 cells were transduced with lentiviruses encoding sgRNA. At 24 h post-transduction, 1 µg/ml puromycin was added for selection for 7 days to generate bulk gene-edited cells. To isolate single cell clones, the lentivirus was transduced into A549 cells for 24 h. Then, cells were transferred to a 10-cm dish and selected using 1 µg/ml puromycin for 7 days. Puromycin-resistant clones were selected and confirmed by Western blotting and genome DNA sequencing.

Genomic DNA of bulk or cloned cells was extracted using a Cell Genomic DNA Extraction kit (Bioteke, Beijing, China). Regions surrounding the sgRNA target sequences were amplified by PCR. PCR products were cloned into pMD-18T (Takara, Kyoto, Japan) for sequencing. Double KO cells were

transduced with two lentiviruses carry sgRNA against each gene and selected as above. The sequencing primers were listed in **Table S2**.

Induction of apoptosis

Cells were transfected with mock or 1 μg/ml poly(I:C) (Sigma, St, Louis, MO, USA) using Lipofectamine 2000 (Invitrogen). Cells were incubated with 3% hydrogen peroxide, 10 μM doxorubicin or 2 μM staurosporine for 24 h.

MTT and CCK8 assay

Cell viability was measured by MTT assay. MTT (Genview, Beijing, China) was added to cell culture (5 mg/ml dissolved in PBS) and incubated for 4 h at 37 °C. After centrifugation at 1500 rpm for 5 min, the supernatant was discarded and DMSO was added to the plate, and gently shaken for 10 min to dissolve the formazan product. OD value was measured at 490 nm using a BioTek Instrument (BioTeke).

Cell Counting Kit-8 (CCK8) was purchased from MCE. The cells were seeded in 12-well plate. 80 μL reagent was added to cell culture at 24 h post-transfection and incubated in the incubator. 1 h later, the OD value was measured at 450 nm using a BioTek Instrument (BioTek).

Generation of HuR-RES, ΔRRM1, ΔRRM2, and ΔRRM3 expressing cells

The full length of *HuR* or the fragment of *HuR* with a deleted RRM1 (*ΔRRM1*), RRM2 (*ΔRRM2*), and RRM3 (*ΔRRM3*) gene was amplified by PCR. Primer sequence were listed in **Table S3**. The

amplified fragments were cloned into the vector CSII-EF-MCS-IRES2-Venus (Riken, Kobe, Japan). The lentivirus was packaged in 293T cells through transfecting CSII-EFMCS-IRES2-Venus-HuR, CSII-EFMCS-IRES2-Venus-ΔRRM1, CSII-EFMCS-IRES2-Venus-ΔRRM2, or CSII-EFMCS-IRES2-Venus-ΔRRM3, pSPAX2 and pMD2.G into cells using FuGENE®HD reagent. After 2 days, the culture supernatant was collected and passed through a 0.45 μm filter for gene transduction. HuR-KO cells were transduced with lentivirus carrying the full length of *HuR*, *ΔRRM1*, *ΔRRM2*, or *ΔRRM3*, and Venus-positive cells were sorted by flow cytometry.

Western blot

Whole cell extracts were prepared in the presence of 1 mM PMSF, 1% (v/v) protease inhibitor cocktail (Sigma) and DDT. Proteins were separated by SDS-PAGE and transferred onto nitrocellulose membranes, followed by blocking in 0.1% PBST with 5% bovine serum albumin (BSA) (New England Biolabs, Massachusetts, USA), and incubating with primary antibodies at 4 °C overnight. Primary antibodies included anti-tubulin (RM2007, BBI Life Science, Shanghai, China), anti-HuR (E0418, Santa Cruz Biotechnology, Texas, USA), anti-PARP (9542, Cell Signaling Technology, Massachusetts, USA) , anti-BCL2 (YM3041, Immunoway, Delaware, USA). Detection was performed with IRDye 800 CW– conjugated anti-rabbit IgG or IRDye 680 LT–conjugated anti-mouse IgG secondary antibody according to the manufacturer's protocols (LI-COR, USA). Immunoreactive bands were visualized using an Odyssey infrared imaging system (LI-COR).

Quantitative reverse transcription-PCR (qRT–PCR)

Total RNAs were reverse transcribed using HI Script Q RT SuperMix (Vazyme, Nanjing, China). qRT-PCR was performed using the cDNA templates and the SYBR Select Master Mix for CFX (Applied Bio systems) in Bio-Rad CFX96 machine. Primers used for qRT-PCR were listed in **Table S4**. The PCR data were analyzed using SDS software (Applied Biosystems). β-actin level was measured as an internal control.

RNA-seq

Total RNA of control and HuR-KO cells was extracted with TRIzol. Three biological replicates were performed. The quality of RNA was detected by using Agilent bioanalyzer 2100. RNA-seq transcriptome library were produced using the NEB Next Ultra RNA library Prep Kit and sequenced on an Illumina NextSeq instrument. R analysis was carried out using the systemPiper workflow. Differential expression analysis was performed using DESeq2 and DEXSeq. Functional-enrichment analysis Kyoto Encyclopedia of Gene and Genomes (KEGG) pathways were compared with the whole-transcriptome background.

mRNA stability assay

Cells were treated with DMSO or 0.5 μg/ml actinomycin D (Act D) (MCE, Shanghai, China) for 2, 4, or 8 h. Total RNA was extracted for cDNA synthesis, and transcript abundances of *BCL2* and *COX2* mRNAs were measured by qRT-PCR.

Flow cytometry analysis

Apoptosis was assessed with PE Annexin V Apoptosis Detection Kit I (Roche, Switzerland) using a flow cytometer (LSRFORTESA, Becton Dickinson, USA). Briefly, A549 cells were stimulated with poly(I:C) for 24 h. The cells were harvested and washed twice in PBS, and then resuspended in 1× binding buffer. 5 μl V-PE and 5 μl 7-AAD were added to 100 μl cell suspension. Next, the mixture was incubated for 15 min at room temperature and resuspended in 1× binding buffer. Labeled cells were analyzed by flow cytometry (BD).

Polysome fractionation

Control and HuR-KO cells were treated with 100 mg/ml cycloheximide at 37 °C for 5 min. Whole cell extracts were prepared and layered onto a 10%-50% continuous sucrose gradient and centrifuged at 39,000 rpm in a Beckman SW-41Ti rotor for 3 h at 4 °C. Samples were collected from the top of the gradient into 12 fractions. Collected fractions were extracted and subjected to qRT-PCR.

Subcellular fractionation assay

Upon indicated treatment, cells were washed twice with PBS and lysed in cytoplasmic extract buffer (10 mm HEPES, 60 mm KCl, 1 mm EDTA, 0.075% (v/v) Nonidet P-40, 1 mm PMSF, and 1 mm DTT). The mixture was spun at 12,000 rpm for 5 min to get the cytoplasmic extract (supernatant). The precipitate was washed with cytoplasmic extract buffer and then lysed in nuclear extract buffer (20 mm

HEPES, 420 mm NaCl, 10 mm KCl, 1 mm PMSF, 1 mm EDTA, and 20% (v/v) glycerol). The mixture was spun at 12,000 rpm for 5 min to get the nuclear extract (supernatant).

Virus, virus infection and titration

The EMCV and SFV were provided by Prof. Rongbin Zhou at University of Science and Technology of China and Prof. Xi Zhou at Wuhan Institute of Virology. EMCV and SFV were propagated in HeLa and C6/36 cells, respectively. The EMCV-infected cells were collected when cytopathic effect appeared and subjected to three cycles of freezing-and-thawing, followed by centrifugation at 1500 rpm for 5 min. The supernatant of SFV-infected cells was collected when cytopathic effect appeared and subjected to centrifugation and filtration. Virus stocks were titered by a standard plaque assay on BHK21 or Vero cells and stored at -80 °C. Serial 10-fold dilutions of virus sample were prepared and inoculated on the cells. The incubation medium was removed and cultured in the mixture of 2×DMEM (Invitrogen) and 2% methylcellulose (Sigma) (1:1). Visible plaques were counted at 2-3 days p.i. (EMCV) or 24 h p.i. (SFV).

For viral infection, A549 cells were incubated with EMCV or SFV at an MOI of 1 for 1 h at 37 °C. At indicated time points post-infection, cells were collected for qRT-PCR, western blot, or flow cytometry detection.

RNA immunoprecipitation assay

Cells were lysed in RIP lysis buffer (100 mM KCl, 5 mM MgCl$_2$, 0.5% [vol/vol] NP-40, 10 mM HEPES, 1 mM PMSF, 1% protease inhibitor cocktails, and RNase inhibitor). Immunoprecipitation was carried out using anti-FLAG M2 Affinity Gel (Sigma). Immune complexes were precipitated with protein A/G agarose as described above. Whole RNA extraction was performed using TRIzol reagent (Invitrogen) according to the manufacturer's protocol. *BCL2*, *ACTIN*, *GAPDH* mRNA levels were analyzed by qRT-PCR (primer sequences were listed in **Table S4**).

Statistical analysis

All experiments were independently repeated at least three times. Comparisons between two groups were performed using ANOVA, ANOVA with Dunnett's multiple comparison test or Student's *t*-tests. Graphs were generated using Graph Pad Prism 6.0 software. P values of 0.05 or lower were considered to be statistically significant.

Data Availability

RNA-Seq data: Gene Expression Omnibus GSE165625

(https://www.ncbi.nlm.nih.gov/geo/query/acc.cgi?acc=GSE165625)

Author contributions

The conceptualization of this project was conducted by Z.L. and Z.P. Investigation was performed by Z.L., G.H.X, L.Y.X., H.C.B., and L.X.B. Formal analysis, visualization, and original draft preparation were performed by Z.L., M.S.D, L.C., and Z.P. The manuscript was reviewed and edited by Z.L., M.D.S, and Z.P. Supervision and project administration were carried out by Z.P. and M.D.S, and funding acquisition was done by Z.P. and L.C. All authors have read and agreed to the published version of the manuscript.

Conflict of interest

M.S.D. is a consultant for Inbios, Vir Biotechnology, NGM Biopharmaceuticals, and Carnival Corporation and on the Scientific Advisory Boards of Moderna and Immunome. The Diamond laboratory has received unrelated funding support in sponsored research agreements from Moderna, Vir Biotechnology, and Emergent BioSolutions. Other authors declare no conflict of interest.

References

Ashkenazi, A., Fairbrother, W. J., Leverson, J. D. and Souers, A. J. (2017). From basic apoptosis discoveries to advanced selective BCL-2 family inhibitors. *Nat Rev Drug Discov* **16**, 273-284.

Badawi, A., Biyanee, A., Nasrullah, U., Winslow, S., Schmid, T., Pfeilschifter, J. and Eberhardt, W. (2018). Inhibition of IRES-dependent translation of caspase-2 by HuR confers chemotherapeutic drug resistance in colon carcinoma cells. *Oncotarget* **9**, 18367-18385.

Balachandran, S., Kim, C. N., Yeh, W. C., Mak, T. W., Bhalla, K. and Barber, G. N. (1998). Activation of the dsRNA-dependent protein kinase, PKR, induces apoptosis through FADD-mediated death signaling. *EMBO J* **17**, 6888-902.

Barber, G. N. (2001). Host defense, viruses and apoptosis. *Cell Death Differ* **8**, 113-26.

Barber, G. N. (2005). The dsRNA-dependent protein kinase, PKR and cell death. *Cell Death Differ* **12**, 563-70.

Bauernfried, S., Scherr, M. J., Pichlmair, A., Duderstadt, K. E. and Hornung, V. (2020). Human NLRP1 is a sensor for double-stranded RNA. *Science*.

Brennan, C. M. and Steitz, J. A. (2001). HuR and mRNA stability. *Cell Mol Life Sci* **58**, 266-77.

Castelli, J. C., Hassel, B. A., Maran, A., Paranjape, J., Hewitt, J. A., Li, X. L., Hsu, Y. T., Silverman, R. H. and Youle, R. J. (1998). The role of 2'-5' oligoadenylate-activated ribonuclease L in apoptosis. *Cell Death Differ* **5**, 313-20.

Chattopadhyay, S. and Sen, G. C. (2017). RIG-I-like receptor-induced IRF3 mediated pathway of apoptosis (RIPA): a new antiviral pathway. *Protein Cell* **8**, 165-168.

Chattopadhyay, S., Yamashita, M., Zhang, Y. and Sen, G. C. (2011). The IRF-3/Bax-mediated apoptotic pathway, activated by viral cytoplasmic RNA and DNA, inhibits virus replication. *J Virol* **85**, 3708-16.

Chawla-Sarkar, M., Lindner, D. J., Liu, Y. F., Williams, B. R., Sen, G. C., Silverman, R. H. and Borden, E. C. (2003). Apoptosis and interferons: role of interferon-stimulated genes as mediators of apoptosis. *Apoptosis* **8**, 237-49.

Danthi, P. (2016). Viruses and the Diversity of Cell Death. *Annu Rev Virol* **3**, 533-553.

Diaz-Guerra, M., Rivas, C. and Esteban, M. (1997). Activation of the IFN-inducible enzyme RNase L causes apoptosis of animal cells. *Virology* **236**, 354-63.

Domingo-Gil, E. and Esteban, M. (2006). Role of mitochondria in apoptosis induced by the 2-5A system and mechanisms involved. *Apoptosis* **11**, 725-38.

Dormoy-Raclet, V., Menard, I., Clair, E., Kurban, G., Mazroui, R., Di Marco, S., von Roretz, C., Pause, A. and Gallouzi, I. E. (2007). The RNA-binding protein HuR promotes cell migration and cell invasion by stabilizing the beta-actin mRNA in a U-rich-element-dependent manner. *Mol Cell Biol* **27**, 5365-80.

El Maadidi, S., Faletti, L., Berg, B., Wenzl, C., Wieland, K., Chen, Z. J., Maurer, U. and Borner, C. (2014). A novel mitochondrial MAVS/Caspase-8 platform links RNA virus-induced innate antiviral signaling to Bax/Bak-independent apoptosis. *J Immunol* **192**, 1171-83.

Erener, S., Petrilli, V., Kassner, I., Minotti, R., Castillo, R., Santoro, R., Hassa, P. O., Tschopp, J. and Hottiger, M. O. (2012). Inflammasome-activated caspase 7 cleaves PARP1 to enhance the expression of a subset of NF-kappaB target genes. *Mol Cell* **46**, 200-11.

Galluzzi, L. Vitale, I. Aaronson, S. A. Abrams, J. M. Adam, D. Agostinis, P. Alnemri, E. S. Altucci, L. Amelio, I. Andrews, D. W. et al. (2018). Molecular mechanisms of cell death: recommendations of the Nomenclature Committee on Cell Death 2018. *Cell Death Differ* **25**, 486-541.

Ghisolfi, L., Calastretti, A., Franzi, S., Canti, G., Donnini, M., Capaccioli, S., Nicolin, A. and Bevilacqua, A. (2009). B cell lymphoma (Bcl)-2 protein is the major determinant in bcl-2 adenine-uridine-rich element turnover overcoming HuR activity. *J Biol Chem* **284**, 20946-55.

Harashima, N., Minami, T., Uemura, H. and Harada, M. (2014). Transfection of poly(I:C) can induce reactive oxygen species-triggered apoptosis and interferon-beta-mediated growth arrest in human renal cell carcinoma cells via innate adjuvant receptors and the 2-5A system. *Mol Cancer* **13**, 217.

He, S., Liang, Y., Shao, F. and Wang, X. (2011). Toll-like receptors activate programmed necrosis in macrophages through a receptor-interacting kinase-3-mediated pathway. *Proc Natl Acad Sci U S A* **108**, 20054-9.

Hinman, M. N. and Lou, H. (2008). Diverse molecular functions of Hu proteins. *Cell Mol Life Sci* **65**, 3168-81.

Hiscott, J., Grandvaux, N., Sharma, S., Tenoever, B. R., Servant, M. J. and Lin, R. (2003). Convergence of the NF-kappaB and interferon signaling pathways in the regulation of antiviral defense and apoptosis. *Ann N Y Acad Sci* **1010**, 237-48.

Imre, G. (2020). Cell death signalling in virus infection. *Cell Signal* **76**, 109772.

Iordanov, M. S., Ryabinina, O. P., Schneider, P. and Magun, B. E. (2005). Two mechanisms of caspase 9 processing in double-stranded RNA- and virus-triggered apoptosis. *Apoptosis* **10**, 153-66.

Ishimaru, D., Ramalingam, S., Sengupta, T. K., Bandyopadhyay, S., Dellis, S., Tholanikunnel, B. G., Fernandes, D. J. and Spicer, E. K. (2009). Regulation of Bcl-2 expression by HuR in HL60 leukemia cells and A431 carcinoma cells. *Mol Cancer Res* **7**, 1354-66.

Jacobs, B. L. and Langland, J. O. (1996). When two strands are better than one: the mediators and modulators of the cellular responses to double-stranded RNA. *Virology* **219**, 339-49.

Jeong, H. H., Kim, S. Y., Rousseaux, M. W. C., Zoghbi, H. Y. and Liu, Z. (2019). Beta-binomial modeling of CRISPR pooled screen data identifies target genes with greater sensitivity and fewer false negatives. *Genome Res* **29**, 999-1008.

Kaufman, R. J. (1999). Double-stranded RNA-activated protein kinase mediates virus-induced apoptosis: a new role for an old actor. *Proc Natl Acad Sci U S A* **96**, 11693-5.

Kibler, K. V., Shors, T., Perkins, K. B., Zeman, C. C., Banaszak, M. P., Biesterfeldt, J., Langland, J. O. and Jacobs, B. L. (1997). Double-stranded RNA is a trigger for apoptosis in vaccinia virus-infected cells. *J Virol* **71**, 1992-2003.

Kullmann, M., Gopfert, U., Siewe, B. and Hengst, L. (2002). ELAV/Hu proteins inhibit p27 translation via an IRES element in the p27 5'UTR. *Genes Dev* **16**, 3087-99.

Li, W., Xu, H., Xiao, T., Cong, L., Love, M. I., Zhang, F., Irizarry, R. A., Liu, J. S., Brown, M. and Liu, X. S. (2014). MAGeCK enables robust identification of essential genes from genome-scale CRISPR/Cas9 knockout screens. *Genome Biol* **15**, 554.

Man, S. M., Karki, R. and Kanneganti, T. D. (2017). Molecular mechanisms and functions of pyroptosis, inflammatory caspases and inflammasomes in infectious diseases. *Immunol Rev* **277**, 61-75.

Okamoto, T., Suzuki, T., Kusakabe, S., Tokunaga, M., Hirano, J., Miyata, Y. and Matsuura, Y. (2017). Regulation of Apoptosis during Flavivirus Infection. *Viruses* **9**.

Orzalli, M. H. and Kagan, J. C. (2017). Apoptosis and Necroptosis as Host Defense Strategies to Prevent Viral Infection. *Trends Cell Biol* **27**, 800-809.

Payne, C. K., Jones, S. A., Chen, C. and Zhuang, X. (2007). Internalization and trafficking of cell surface proteoglycans and proteoglycan-binding ligands. *Traffic* **8**, 389-401.

Sanjana, N. E., Shalem, O. and Zhang, F. (2014). Improved vectors and genome-wide libraries for CRISPR screening. *Nat Methods* **11**, 783-784.

Scallan, M. F., Allsopp, T. E. and Fazakerley, J. K. (1997). bcl-2 acts early to restrict Semliki Forest virus replication and delays virus-induced programmed cell death. *J Virol* **71**, 1583-90.

Sengupta, S., Jang, B. C., Wu, M. T., Paik, J. H., Furneaux, H. and Hla, T. (2003). The RNA-binding protein HuR regulates the expression of cyclooxygenase-2. *J Biol Chem* **278**, 25227-33.

Son, K. N., Liang, Z. and Lipton, H. L. (2015). Double-Stranded RNA Is Detected by Immunofluorescence Analysis in RNA and DNA Virus Infections, Including Those by Negative-Stranded RNA Viruses. *J Virol* **89**, 9383-92.

Takeuchi, O. and Akira, S. (2009). Innate immunity to virus infection. *Immunol Rev* **227**, 75-86.

Upton, J. W., Shubina, M. and Balachandran, S. (2017). RIPK3-driven cell death during virus infections. *Immunol Rev* **277**, 90-101.

Urban, C., Rheme, C., Maerz, S., Berg, B., Pick, R., Nitschke, R. and Borner, C. (2008). Apoptosis induced by Semliki Forest virus is RNA replication dependent and mediated via Bak. *Cell Death Differ* **15**, 1396-407.

Wannamaker, W., Davies, R., Namchuk, M., Pollard, J., Ford, P., Ku, G., Decker, C., Charifson, P., Weber, P., Germann, U. A. et al. (2007). (S)-1-((S)-2-{[1-(4-amino-3-chloro-phenyl)-methanoyl]-amino}-3,3-dimethyl-butanoyl)-pyrrolidine-2-carboxylic acid ((2R,3S)-2-ethoxy-5-oxo-tetrahydro-furan-3-yl)-amide (VX-765), an orally available selective interleukin (IL)-converting enzyme/caspase-1 inhibitor, exhibits potent anti-inflammatory activities by inhibiting the release of IL-1beta and IL-18. *J Pharmacol Exp Ther* **321**, 509-16.
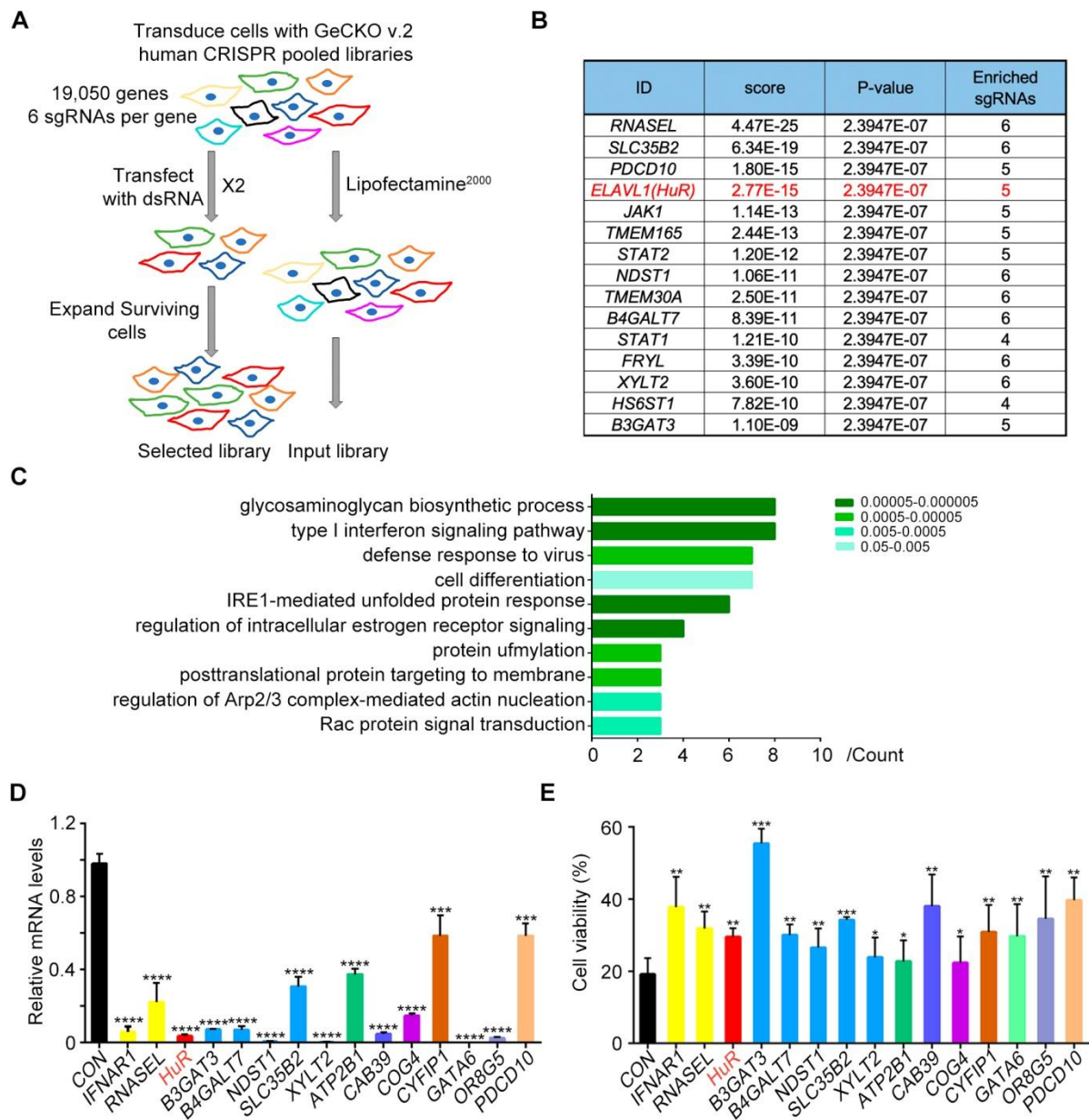
Winkler, C., Doller, A., Imre, G., Badawi, A., Schmid, T., Schulz, S., Steinmeyer, N., Pfeilschifter, J., Rajalingam, K. and Eberhardt, W. (2014). Attenuation of the ELAV1-like protein HuR sensitizes adenocarcinoma cells to the intrinsic apoptotic pathway by increasing the translation of caspase-2L. *Cell Death Dis* **5**, e1321.

Zhang, Z., Yao, Z., Wang, L., Ding, H., Shao, J., Chen, A., Zhang, F. and Zheng, S. (2018). Activation of ferritinophagy is required for the RNA-binding protein ELAVL1/HuR to regulate ferroptosis in hepatic stellate cells. *Autophagy* **14**, 2083-2103.

Zhou, A., Paranjape, J., Brown, T. L., Nie, H., Naik, S., Dong, B., Chang, A., Trapp, B., Fairchild, R., Colmenares, C. et al. (1997). Interferon action and apoptosis are defective in mice devoid of 2',5'-oligoadenylate-dependent RNase L. *EMBO J* **16**, 6355-63.
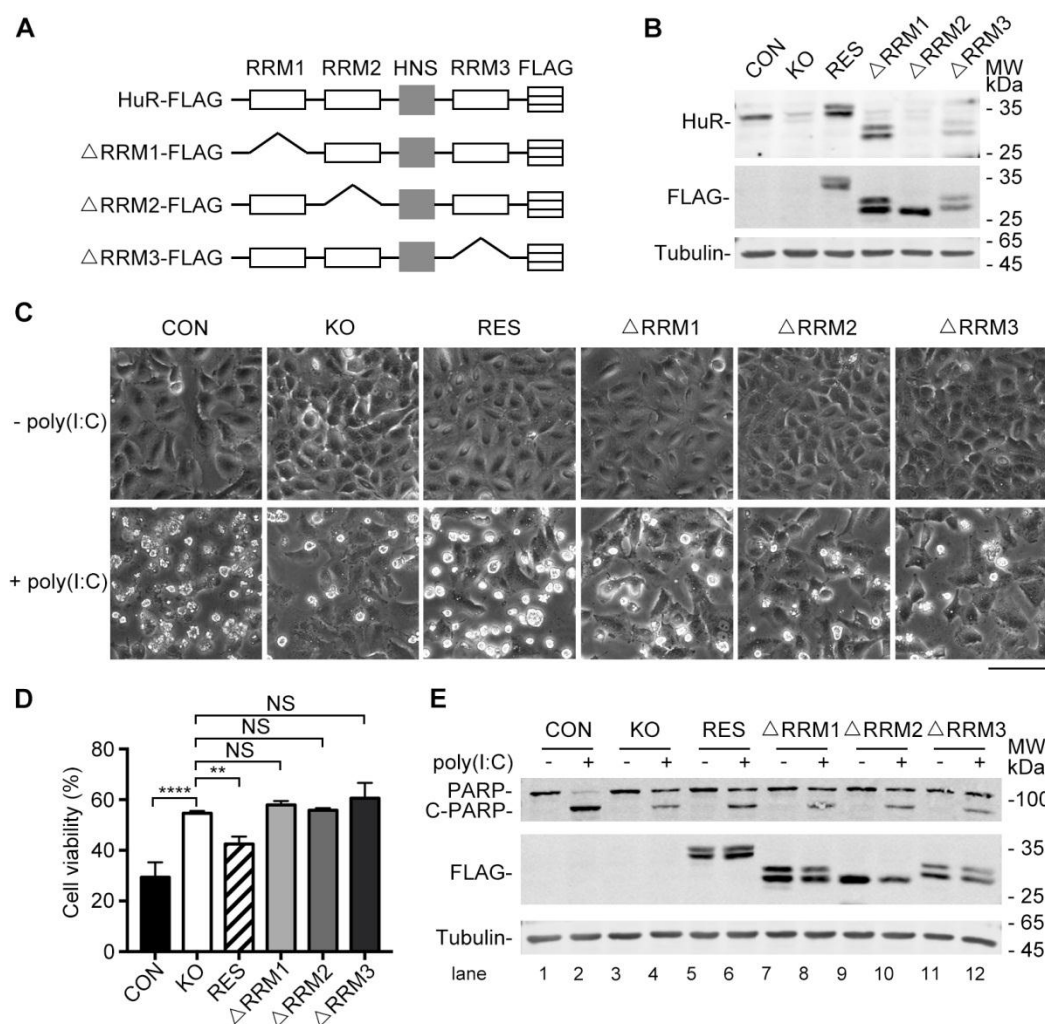
Figures

A — Transduce cells with GeCKO v.2 human CRISPR pooled libraries

19,050 genes
6 sgRNAs per gene

Transfect with dsRNA X2 / Lipofectamine^2000

Expand Surviving cells

Selected library   Input library

B

ID	score	P-value	Enriched sgRNAs
RNASEL	4.47E-25	2.3947E-07	6
SLC35B2	6.34E-19	2.3947E-07	6
PDCD10	1.80E-15	2.3947E-07	5
ELAVL1(HuR)	2.77E-15	2.3947E-07	5
JAK1	1.14E-13	2.3947E-07	5
TMEM165	2.44E-13	2.3947E-07	5
STAT2	1.20E-12	2.3947E-07	5
NDST1	1.06E-11	2.3947E-07	6
TMEM30A	2.50E-11	2.3947E-07	6
B4GALT7	8.39E-11	2.3947E-07	6
STAT1	1.21E-10	2.3947E-07	4
FRYL	3.39E-10	2.3947E-07	6
XYLT2	3.60E-10	2.3947E-07	6
HS6ST1	7.82E-10	2.3947E-07	4
B3GAT3	1.10E-09	2.3947E-07	5

C

glycosaminoglycan biosynthetic process
type I interferon signaling pathway
defense response to virus
cell differentiation
IRE1-mediated unfolded protein response
regulation of intracellular estrogen receptor signaling
protein ufmylation
posttranslational protein targeting to membrane
regulation of Arp2/3 complex-mediated actin nucleation
Rac protein signal transduction

Legend: 0.00005-0.000005 / 0.0005-0.00005 / 0.005-0.0005 / 0.05-0.005

/Count (0, 2, 4, 6, 8, 10)

D — Relative mRNA levels (CON, IFNAR1, RNASEL, HuR, B3GAT3, B4GALT7, NDST1, SLC35B2, XYLT2, ATP2B1, CAB39, COG4, CYFIP1, GATA6, OR8G5, PDCD10)

E — Cell viability (%) (CON, IFNAR1, RNASEL, HuR, B3GAT3, B4GALT7, NDST1, SLC35B2, XYLT2, ATP2B1, CAB39, COG4, CYFIP1, GATA6, OR8G5, PDCD10)

Figure 1. CRISPR/Cas9 genetic screen identifies genes involved in dsRNA-induced cell death. (**A**) Scheme summarizing the screening strategy. (**B**) Top-ranking genes showing the gene identifier (ID), score, P-value, and number of enriched sgRNA as calculated by MAGeCK analysis. The screen was performed three independent times. (**C**) DAVID analysis of common regulated genes. Colors indicate P values. (**D**) Efficiency of gene-editing. Total mRNAs of the bulk gene-edited A549 cells were extracted for qRT-PCR analysis. (**E**) Validation assay. Gene-edited A549 cells were transfected with poly(I:C) for 24 h, and cell viability was determined by an MTT assay. Data were mean ± standard deviation (SD) from three independent experiments performed in two replicates. P values were calculated by ANOVA with Dunnett's multiple comparison test (*$P < 0.05$, **$P < 0.01$, ***$P < 0.001$).
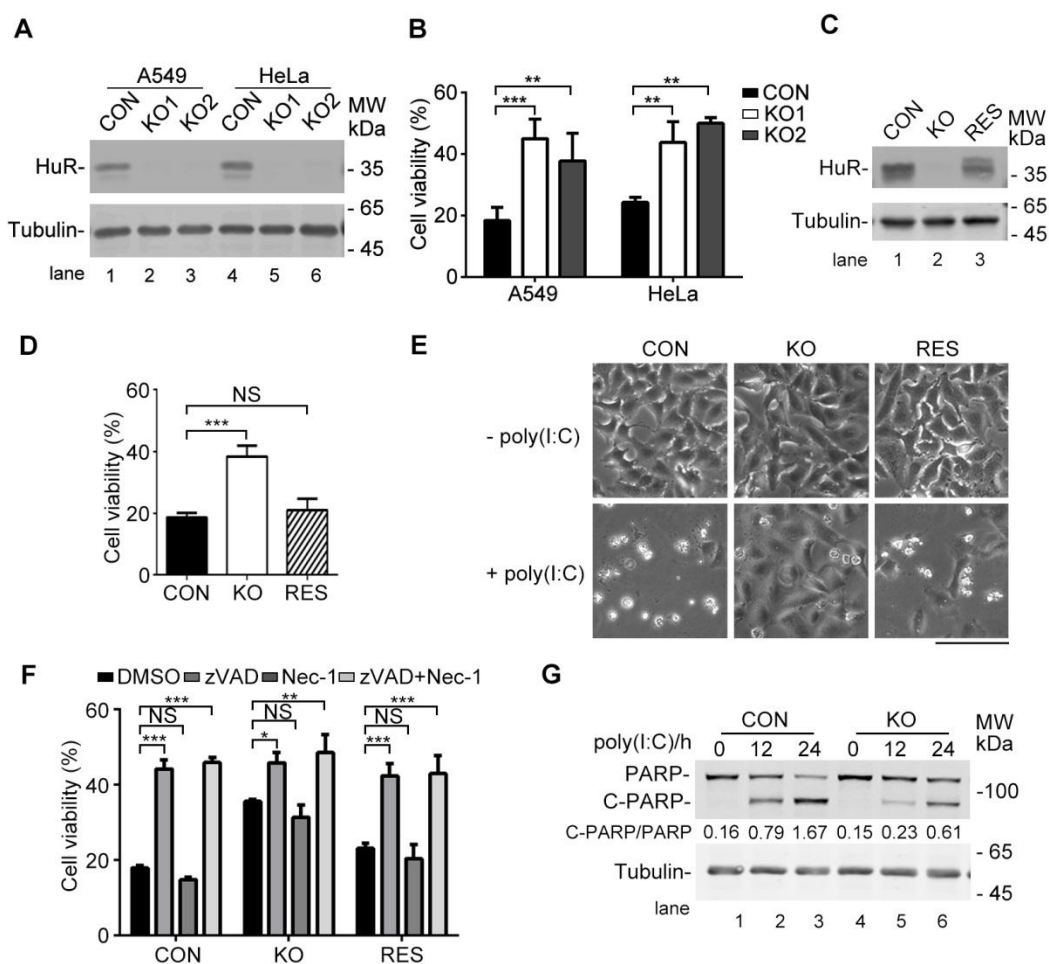
Figure 2. HuR promotes dsRNA-induced cell death. (**A**) Western blotting analysis showing the levels of HuR in control (CON) A549 and HeLa cells, and HuR-knockout (KO) cells. Tubulin was probed as a loading control. Data are representative of three experiments. (**B**) Control cells and HuR-KO cells were transfected with poly(I:C) for 24 h, and cell viability was measured by MTT assay. Data were mean ± SD from three independent experiments with two replicates. P values were calculated by ANOVA with Dunnett's multiple comparison test (**P< 0.01, ***P< 0.001). (**C**) Western blot analysis of HuR levels in control, HuR-KO, and HuR complemented cells (RES). Data were representative of three experiments. (**D, E**) Control, HuR-KO, and HuR-RES cells were transfected with poly(I:C). At 24 h post transfection, cell viability was measured by MTT assay (**D**) and cell images were acquired (**E**). Scale bar, 100 μm.

Data were mean ± SD from three independent experiments. P values were calculated by ANOVA with Dunnett's multiple comparison test (NS, no statistical significance, ***P< 0.001). (**F**) Control, HuR-KO, HuR-RES cells were pretreated with z-VAD(OMe)-FMK (zVAD), Necrostatin-1 (Nec-1) or their combination for 1 h, followed by transfection with poly(I:C) for 24 h. Cell viability was measured by MTT assay. Data were mean ± SD from three independent experiments with two replicates. P values were calculated by ANOVA with Dunnett's multiple comparison test (NS, no statistical significance, *P< 0.05, **P< 0.01, ***P< 0.001). (**G**) Cells were transfected with poly(I:C). At 12 and 24 h post-transfection, cells were harvested for Western blotting to detect the levels of PARP and cleaved PARP (C-PARP). Data were representative of three experiments.

Figure 3. All three RRM domains are required for HuR-mediated apoptosis. (**A**) Schematic representation of HuR and truncate HuR (ΔRRM1, ΔRRM2, and ΔRRM3). (**B**) Western blotting to show the protein levels of HuR in the control, HuR-KO, HuR-RES, and HuR-KO cells expressing ΔRRM1-FLAG (ΔRRM1), ΔRRM2-FLAG (ΔRRM2), and ΔRRM3-FLAG (ΔRRM3). Data were representative of three experiments. (**C, D**) Cells were transfected with poly(I:C). At 24 h post-transfection, cell images were captured (C), and cells were subjected to MTT assay to measure cell viability (D). Representative images of three independent experiments were shown. Scale bar, 100 μm.

Data were mean ± SD from three independent experiments. P values were calculated by ANOVA with Dunnett's multiple comparison test (NS, no statistical significance, **P< 0.01, ****P< 0.0001). (**E**) Cells were transfected with poly(I:C). At 12 h post-transfection, cells were harvested for Western blotting to detect the levels of PARP and cleaved PARP (C-PARP). Data were representative of three experiments.
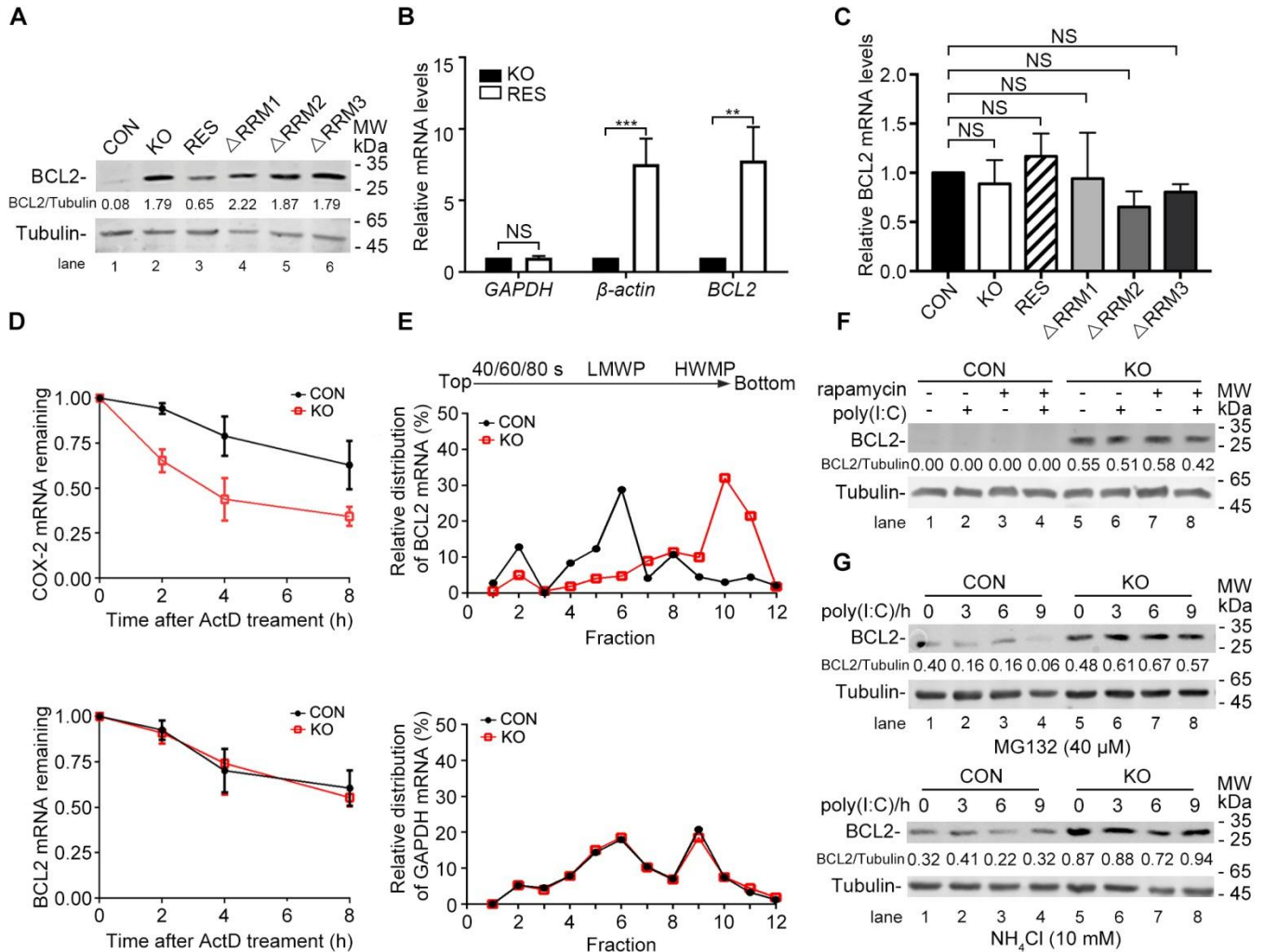
Figure 4. HuR inhibits the translation of BCL2. (**A**) Western blotting analysis of BCL2 levels in control, HuR-KO, HuR-RES, ΔRRM1, ΔRRM2, and ΔRRM3 cells. Tubulin was probed as a loading control. Data were representative of three experiments. (**B**) RNA immunoprecipitation (RIP) assay. Whole cell lysates of HuR-KO and HuR-RES cells were subjected to immunoprecipitation using anti-FLAG antibody. Total RNAs in the precipitates were extracted for qRT-PCR to measure the *BCL2*, *GAPDH*, and *β-actin* mRNA levels. The values were depicted as -fold change compared with the corresponding mRNA levels in HuR-KO cells. Data were mean ± SD from three independent

experiments. P values were calculated by unpaired, two-tailed student's test; ***p < 0.001, **p < 0.01, and NS, no statistical significance. (**C**) Analysis of *BCL2* mRNA levels of control, HuR-KO, HuR-RES, ΔRRM1, ΔRRM2, and ΔRRM3 cells. Total RNAs were subjected to qRT-PCR to measure levels of *BCL2* mRNA. Data were mean ± SD from three independent experiments with two replicates. P values were calculated by ANOVA with Dunnett's multiple comparison test (NS, no statistical significance). (**D**) mRNA stability assay. Cell transcription was blocked by actinomycin D. At the indicated time points, cellular RNAs were extracted for qRT-PCR. The mRNA levels of *COX-2* (*left*) or *BCL2* (*right*) measured immediately before the addition of actinomycin D were set as 1. Data were mean ± SD from three independent experiments. P values were calculated by Kruskal-Wallis ANOVA (NS, no statistical significance, **P< 0.01, ***P< 0.001). (**E**) Polysome fraction analysis. Control and HuR-KO cells were fractionated into cytoplasmic extracts after sucrose gradient centrifugation. The distribution of *BCL2* mRNAs was quantified by qRT-PCR analysis of RNA isolated from 12 gradient fractions. (LMWP: low molecular weight polysomes; HMWP: high molecular weight polysomes). (**F**) HuR is not involved in the cap-dependent translation of BCL2. Control and HuR-KO cells were pretreated with rapamycin for 1 h, followed by transfection with poly(I:C) for 24 h. Whole cell lysates were harvested for detection of BCL2. Tubulin was probed as an internal control. Representative blots of three independent experiments were presented.(**G**) Effect of HuR on the post-transcriptional regulation of *BCL2*. Cells were treated with MG132 (proteasome inhibitor) or with NH_4Cl (lysosome inhibitor). At indicated time points, cells were subjected to Western blotting analysis of BCL2 protein. Data were representative of three experiments.
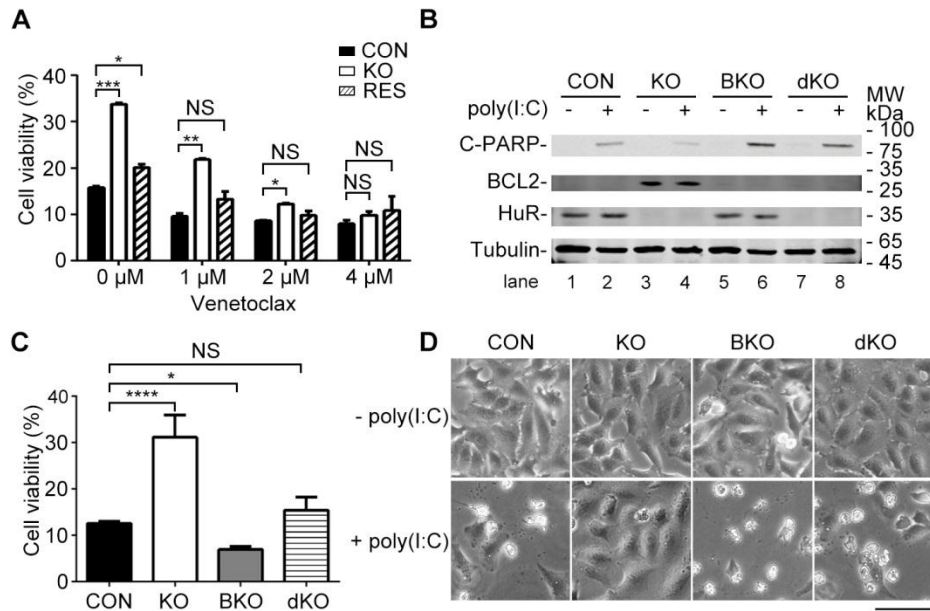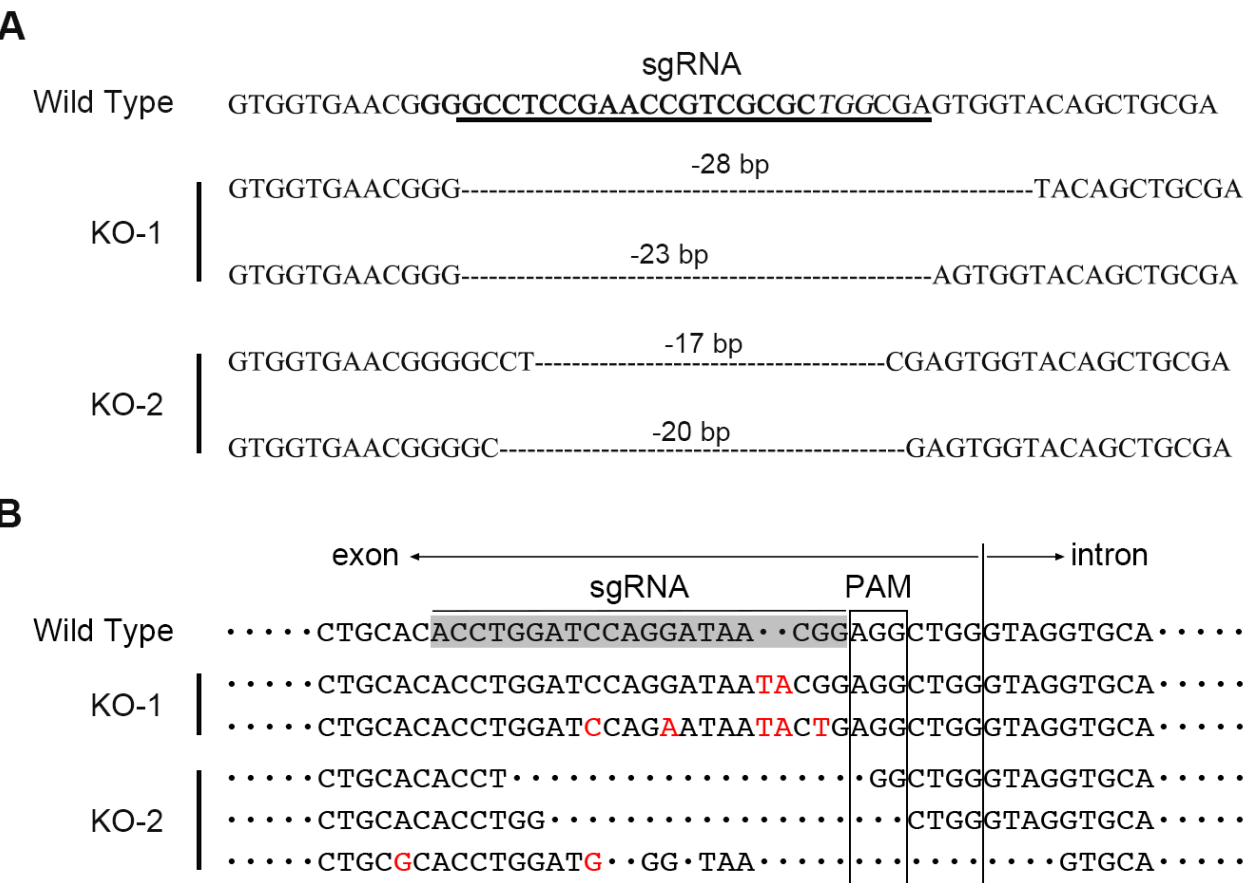
Figure 5. Role of BCL2 in HuR-mediated apoptosis. (**A**) Inhibitor assay. Control, HuR-KO, and HuR-RES cells were pretreated with vehicle or venetoclax at indicated concentrations, followed by transfection with poly(I:C) for 24 h. Cell viability was measured by MTT assay. Data were mean ± SD from three independent experiments. P values were calculated by ANOVA with Dunnett's multiple comparison test (NS, no statistical significance, *P< 0.05, **P< 0.01, ***P< 0.001). (**B**) Western blotting. Tubulin was probed as an internal control. Whole cell lysates of control cells, HuR-KO, BCL2-KO (BKO), and HuR/BCL2 double knockout (dKO) cells were prepared for detection of BCL2, HuR and C-PARP. Data were representative of three independent experiments. (**C, D**) Cell viability and cell images. The control, HuR-KO, BCL2-KO (BKO), and dKO cells were transfected with poly(I:C), and harvested at 24 h post transfection for MTT assay (**C**) or for morphologic analysis (**D**). Scale bar, 100 μm. Data were mean ± SD from three independent experiments. P values were calculated by ANOVA with Dunnett's multiple comparison test (NS, no statistical significance, *P< 0.05, ****P< 0.0001).
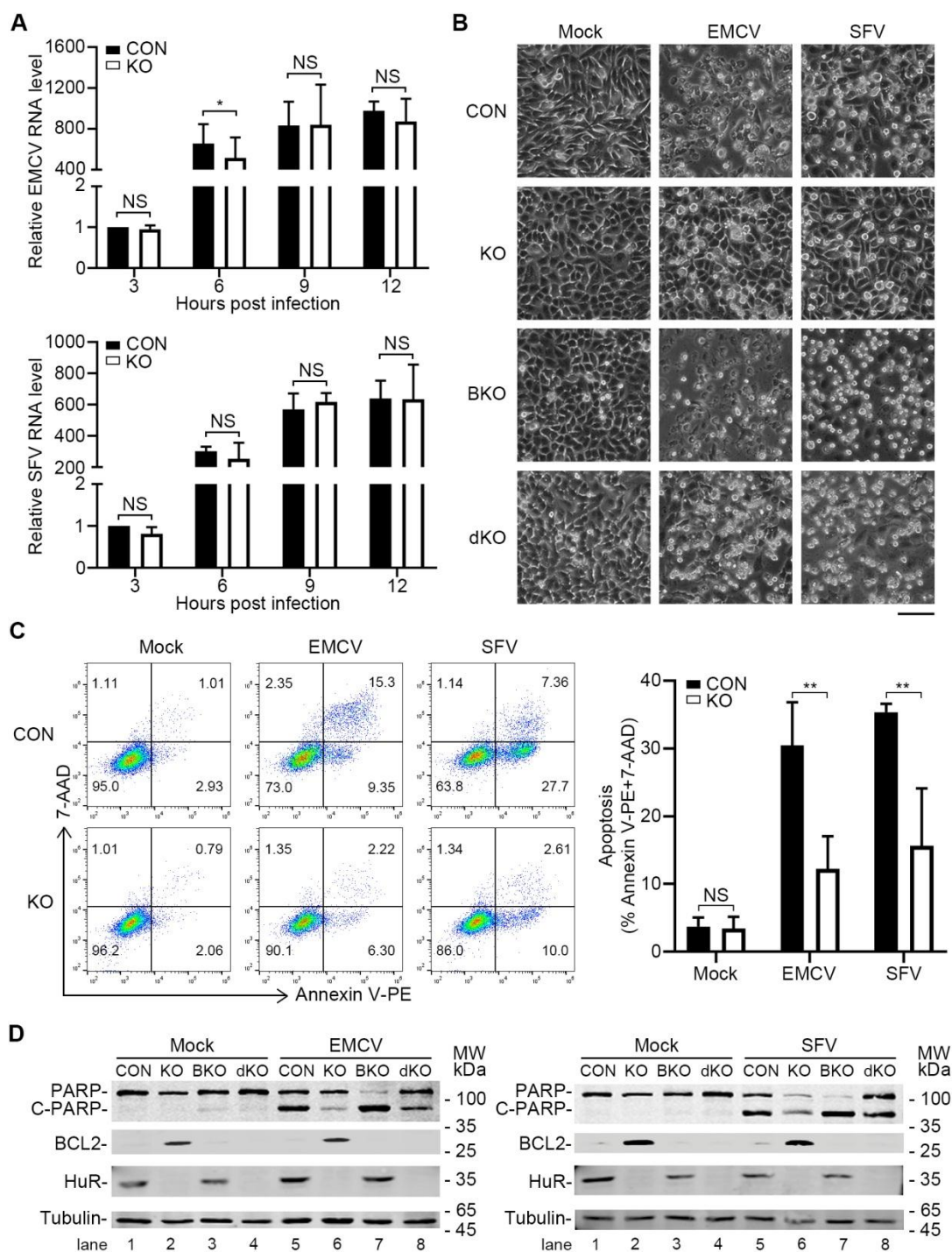
Figure 6. HuR contributes to virus-induced apoptosis. Control and HuR-KO cells were infected with EMCV or SFV at an MOI of 1, and at indicated time points, cells were harvested for analysis of viral RNA levels **(A)**. At 3, 6, 9, and 12 h p.i., total RNAs were harvested for qRT-PCR to determine the EMCV or SFV RNA levels. The data were presented as mean ± SD from three experiments; P values were calculated by unpaired, two-tailed Student's t test (NS, not significant and $*p < 0.05$). **(B)** Cell images were taken at 24 h p.i.; representative images of three independent experiments were shown. Scale bar, 100 μm. **(C)** Flow cytometry analysis. At 24 h p.i., the control and HuR-KO cells were collected for flow cytometry after staining with Annexin V-PE and 7-AAD. Representative data of three independent experiments were shown. The data were presented as mean ± SD from three experiments; P values were caculated by unpaired, two-tailed Student's t test (NS, not significant and $**p < 0.01$). **(D)** Western blotting. At 24 h p.i., the cells were harvested for detection of PARP and C-PARP levels. Tubulin was probed as an internal control. Data were representative of three experiments.
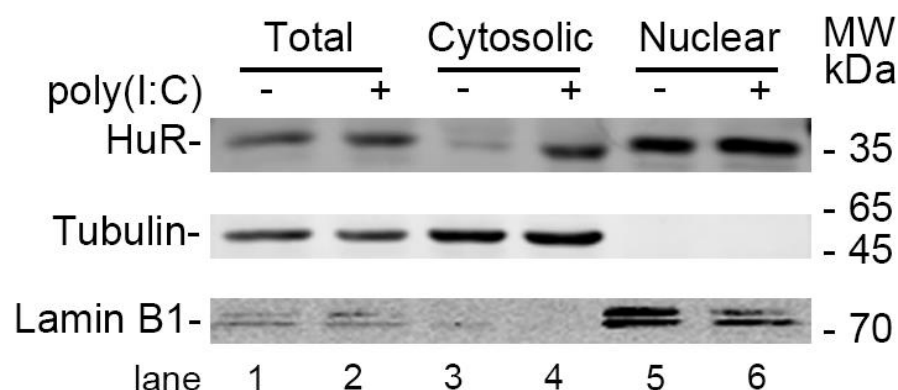
Fig. S1.   **HuR is partially transported into cytoplasm upon dsRNA stimulation.** A549 cells were transfected with poly(I:C). At 12 h post-transfection, cells were harvested for protein fractionation. Proteins derived from cytoplasmic fractions and nuclear fractions were subjected to western blot. Tubulin and Lamin B1 were probed as the loading control for the cytoplasmic fraction and nuclear fraction respectively. Data were representative of three independent experiments.

A

sgRNA

Wild Type   GTGGTGAACG**GGGCCTCCGAACCGTCGCGC***TGG*CGAGTGGTACAGCTGCGA

KO-1

-28 bp
GTGGTGAACGGG--TACAGCTGCGA

-23 bp
GTGGTGAACGGG---AGTGGTACAGCTGCGA

KO-2

-17 bp
GTGGTGAACGGGGCCT--------------------------------------CGAGTGGTACAGCTGCGA

-20 bp
GTGGTGAACGGGGC-------------------------------------GAGTGGTACAGCTGCGA

B

exon ←   → intron

sgRNA   PAM

Wild Type   ·····CTGCAC<mark>ACCTGGATCCAGGATAA</mark>··CGGAGGCTGGGTAGGTGCA·····

KO-1

·····CTGCACACCTGGATCCAGGATAA**TA**CGGAGGCTGGGTAGGTGCA·····

·····CTGCACACCTGGAT**C**CAG**A**ATAA**TACT**GAGGCTGGGTAGGTGCA·····

KO-2

·····CTGCACACCT··················GGCTGGGTAGGTGCA·····

·····CTGCACACCTGG················CTGGGTAGGTGCA·····

·····CTGC**G**CACCTGGAT**G**··GG·TAA····························GTGCA·····

Fig. S2. Confirmation of *ELAVL1*(*HuR*) or *BCL2* knockout efficiency.(**A**) Genomic DNA sequences of HuR KO cell clones (HuR-KO1 and HuR-KO2). Genomic DNA was extracted, and the region surrounding sgRNA targeting *HuR* sequences was amplified by PCR for sequencing. (**B**) Genomic DNA sequences of HuR and BCL2 double knockout cells (dKO1 and dKO2). A549 cells has three copies of *HuR* gene and three copies of *BCL2* gene. Genomic DNA was extracted, and the region surrounding sgRNA targeting *BCL2* sequences was amplified by PCR for DNA sequencing.
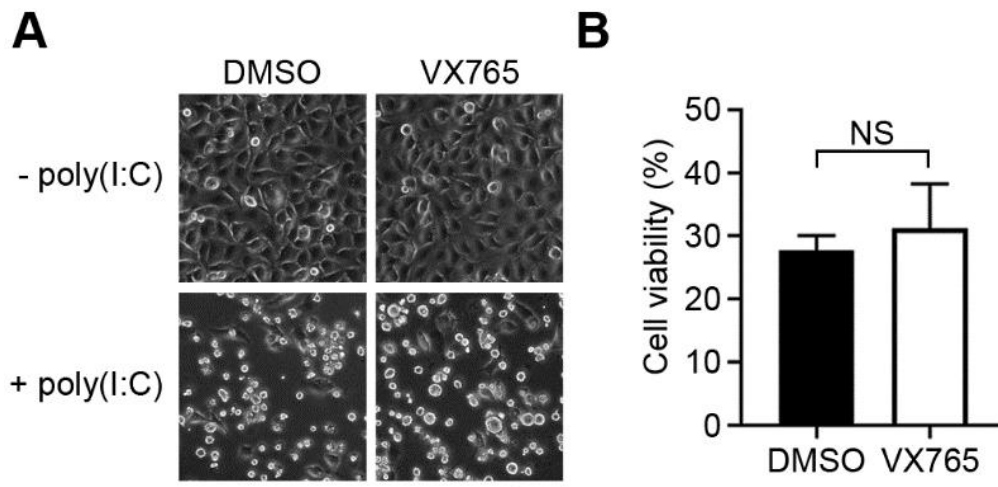
Fig. S3. Poly(I:C) does not trigger pyroptosis in A549 cells. **(A, B)** A549 cells were pretreated with VX765 for 1 h, followed by transfection with 1 μg/ml of poly(I:C) for 24 h. Cell viability was measured by CCK8 assay **(A)** and cell images were captured **(B).** Scale bar, 100 μm. Data were mean ± SD from three independent experiments. P values were calculated by ANOVA with Dunnett's multiple comparison test; NS, no statistical significance.
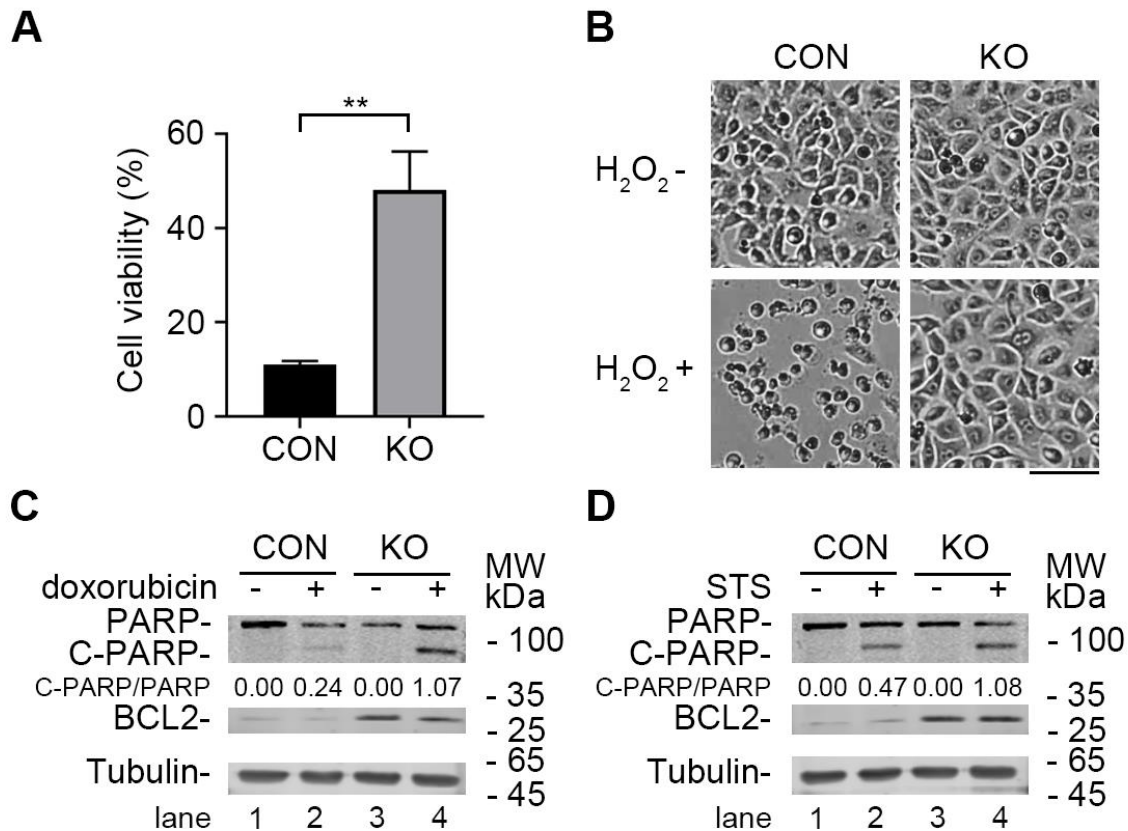
Fig. S4. HuR plays differential roles in apoptosis induced by hydrogen peroxide, doxorubicin or staurosporine. Control and HuR-KO cells were treated with hydrogen peroxide, doxorubicin or staurosporine for 24 h. Cell viability of cells treated with hydrogen peroxide was measured by MTT assay **(A)** and cell images were captured **(B)**. Cells treated with doxorubicin **(C)** or staurosporine **(D)** were harvested for western blotting. Whole cells lysates were harvested for detection of PARP and cleaved PARP (C-PARP) levels. Tubulin was probed as an internal control. Representative data of three independent experiments were shown. The data were presented as mean ±SD from three experiments; P values were calculated by unpaired, two-tailed Student's t test (NS, not significant and **p < 0.01). Scale bar, 100 μm.
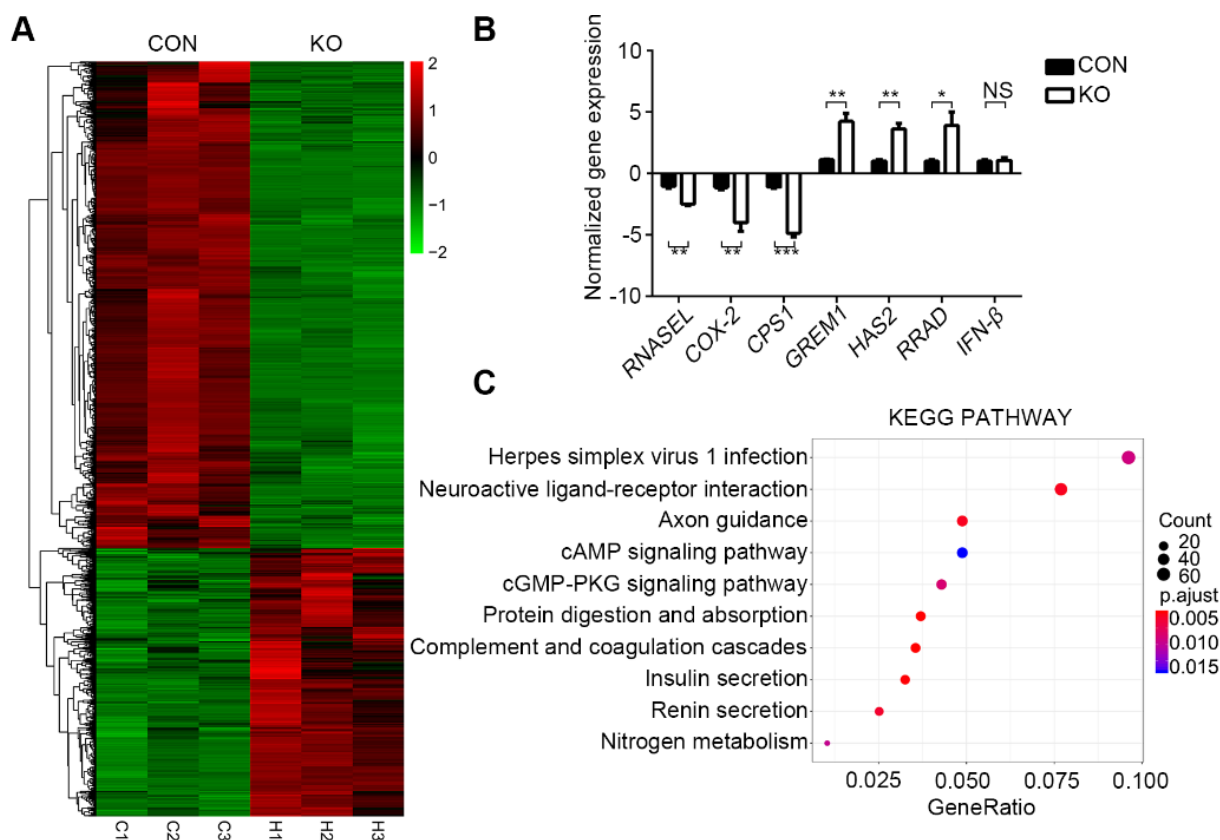
Fig. S5. Transcriptional profiling of control and HuR KO cells. (**A**) Heatmap of mRNA level changes for differentially expressed genes in control and HuR-KO cells at baseline. Heatmap colors represent the ratio of regulated genes. Red and green correspond to over- and under-represented, respectively. C1-3 and H1-3 represent three biological replicates in control and HuR-KO cells. (**B**) Verification of selected genes identified in RNA-seq analysis by qRT-PCR. The y-axis represents the fold changes of HuR-KO cells transcripts normalized to control cells. Data are mean $\pm$ SD from three independent experiments. P values were calculated by unpaired, two-tailed Student's *t*-test; NS, no statistical significance, *P< 0.05, **P< 0.01, ***P< 0.0001. (**C**) Kyoto Encyclopedia of Genes and Genomes (KEGG) enrichment analysis of differentially-expressed genes (DEGs) in control and HuR-KO cells. The x-axis represents the proportion of the targets accounted for all genes of a specific pathway term. The y-axis represents enrichment KEGG pathways. The size of the point represents the gene count in this item.
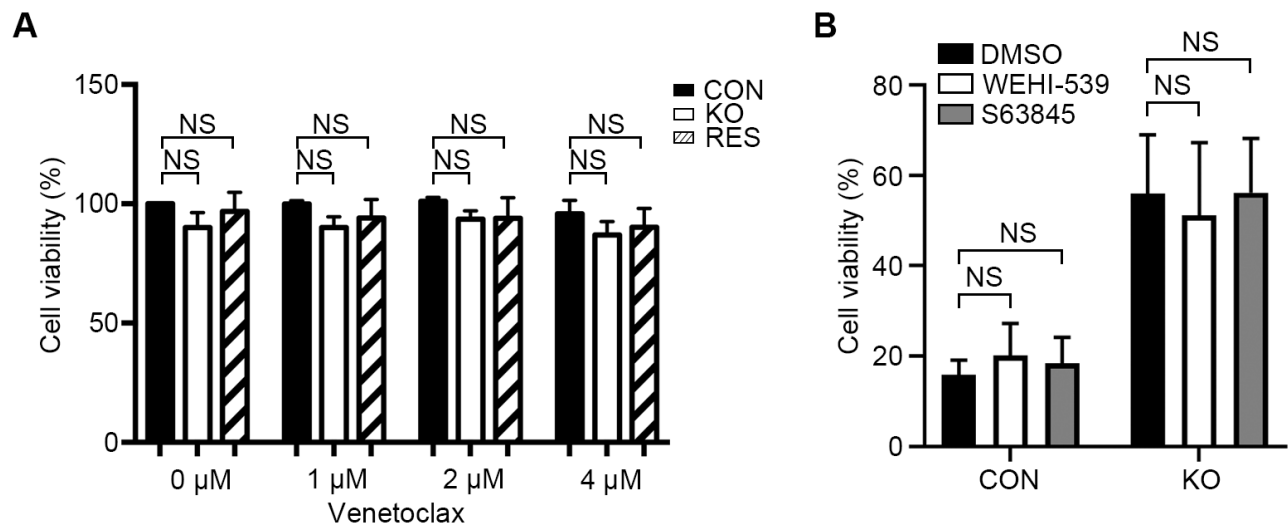
Fig. S6. Role of Bcl-2 members in the HuR-mediated apoptosis. (A) Effect of Bcl-2 inhibitor Venetoclax on the cell viability. Control, HuR-KO, and HuR-RES were treated with 0, 1, 2, or 4 µM Ventoclax for 24 h. Cell viability was measured by MTT assay. P values were calculated by unpaired, two-tailed Student's *t*-test. NS, not significant. **(B)** Role of Bcl-XL and Mcl-1 in the HuR-mediated apoptosis. Control and HuR-KO cells were pretreated with DMSO, WEHI-539 (an inhibitor of Bcl-XL) or S63845 (an inhibitor of Mcl-1) for 1 h, followed by transfection with poly(I:C) for 24 h. Cell viability was measured by CCK8 assay. Data are mean ± SD from three independent experiments. P values were calculated by ANOVA with Dunnett's multiple comparison test; NS, no statistical significance.

Table S1. Sequences of sgRNAs

Genes	sgRNA sequence
ATP2B1	CCACACACACTACAGACAAG
B3GAT3	TTCCCTTACCCGAGTGCAGT
B4GALT7	CAGCAGGATGCCGCCGACAT
CAB39	GTGCAGATGTATTCAACAGT
COG4	TCTAGGGATTGCCCGCATTG
CYFIP1	AATCTACGAGAAAACCGTGG
ELAVL1(HuR)	GGGCCTCCGAACCGTCGCGC
IFNAR	TCATTTACACCATTTCGCAA
GATA6	AGCCGCAGTTCACGCACTCG
NDST1	CGTGCACGTGCAGCTGTACG
OR8G5	ATTTGTGCGTCAGCTCATAT
PDCD10	AATATCAATACCAGAACCGC
RNASEL	GCAGATCACCCACAGTGTTC
SLC35B2	TCCGCCTGAAGTACTGCACC
XYLT2	GGTGCGAATCGCCTACATGC

Table S2. Sequences of primers used in DNA sequencing

Genes		Sequences (5'-3')
HuR	5F	AGTGCAGTGGTATGATCACAA
	3R	CCGGGAAGAAAGTCTGAAGC
BCL2	5F	GAACAGGGTACGATAACCGGG
	3R	TCTCCACGACTAGCAAGCAA

Table S3. Sequences of primers used in amplification of *HuR* gene fragments.

Genes		Sequences (5'-3')
HuR	5F	ATAAGAATGCGGCCGCATGGTGGGCAGTGGTGGTGCTG
	3R	GCGGGATCCTCAAACCTTCTGCACAGGAGAC
HuR-ΔRRM1	5F	ATTGCGGCCGCATGAGCTGAGAGGTGATCAAAGA
	3R	GGGAGGGAGAGGGGCGGATCCTTATTTGTGGGACTTGTTGG
HuR-ΔRRM2	Former-5F	ACGCTACCGGTCTCGAGAATTCATGTCTAATGGTTATGAAGA
	Former-3R	ACGTTTTTGTTCTGGTTGGGGTCTTTGATCACCTCTGAGC
HuR-ΔRRM2	Latter-5F	CCCAACCAGAACAAAAACGT
	Latter-3R	GGGAGGGAGAGGGGCGGATCCTTATTTGTGGGACTTGTTGG
HuR-ΔRRM3	5F	ATAAGAATGCGGCCGCATGGTGGGCAGTGGTGGTGCAGGCTG AAGTGCTTCAGGTTCAGGTTAGGCAAGTGCTG
	3R	ATTGGTCACTTCAGGTTGCTACCGTGCTAGCTAGCTACCGTGC TG

Table S4. Sequences of primers used in qRT-PCR.

Genes		Sequences (5'-3')
BCL2	5F	GGTGGGGGTCATGTGTGTGG
	3R	CGGTTCAGGTACTCAGTCATCC
BAX	5F	CCCGAGAGGTCTTTTTCCGAG
	3R	CCAGCCCATGATGGTTCTGAT
β-Actin	5F	GCTCCTCCTGAGCGCAAG
	3R	CATCTGCTGGAAGGTGGACA
GAPDH	5F	GCCTTCCGTGTCCCCACTG
	3R	CGCCTGCTTCACCACCTTC
COX-2	5F	TTCAAATGAGATTGTGGGAAAATTGCT
	3R	AGATCATCTCTGCCTGAGTATCTT
EMCV	5F	AATGCCCACTACGCTGGT
	3R	GTCGTTCGGCAGTAGGGT
SFV	5F	CCGGAGGACGCACAGAAGTTG
	3R	TGCGACGGCCACAATCGGAAG